Author:
Holmes, Rae-Darcia

Title:
Nitrogen-Doped Diamond

A Thermionic Investigation on the Effects of Lithium Oxide Termination

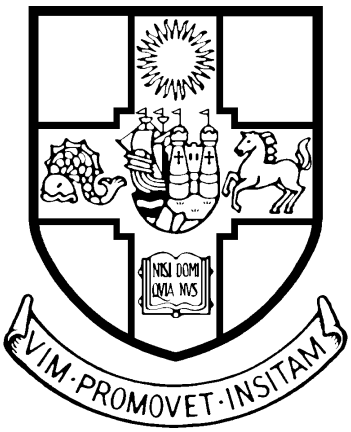

Nitrogen-Doped Diamond; A Thermionic Investigation on the Effects of Lithium Oxide Termination

Rae-Darcia Holmes

September 2023

Supervisor: Professor Neil Fox
Secondary Supervisor: Martin Cryan

A dissertation submitted to the University of Bristol
in accordance with the requirements for award of the degree of
MScR in the faculty of Physics.

School of Physics
UNIVERSITY of BRISTOL

Abstract

This project aims to investigate the emission currents produced from nitrogen-doped diamond samples terminated with oxygen and lithium, to develop our understanding of such a material for use as an emitter surface in a thermionic energy converter (TEC). Thermionic devices offer clean, renewable energy generation from a device with no moving parts thus a large potential for device efficiency, such a device could be revolutionary for electricity generation using solar power, or for clean hydrogen production from electrolysis. TECs could also be used for space-based solar power or energy generation for space travel due to the high physical and radiation hardness of diamond. For an effective TEC device, the semiconductor emitter surface must exhibit a negative electron affinity (NEA) for electron emission, as well as a low work function (WF) to reduce the operating temperatures of such a thermal device.

Nitrogen is a deep-level electron donor when used as a diamond dopant, it easily incorporates into the diamond lattice through substitutional sites. Lithium terminations have been studied both theoretically and experimentally to both induce an NEA and to reduce the work function by inducing dipoles on the surface of the diamond films, altering the semiconductor's band structure through electrostatic band bending.[1,2,3] Oxygenation has shown to increase the bond strength of lithium to the surface as well as that of the surface dipoles, further reducing the WF.[2,4,2]

Diamond films have been grown using chemical vapour deposition (CVD) in nitrogen-rich environments, the effects of changing nitrogen flow rates within the gaseous growth mixture have been investigated in terms of sample quality and electronic properties of the resulting sample. Oxygenation will be used to increase the stability of the terminated lithium surface as well as to further reduce the resulting WF, these terminations have been carried out by UVO-cleaning treatments and thermal evaporation respectively.

X-ray photoemission spectroscopy (XPS) has been used to identify surface contaminants as well as to calibrate lithium deposition rates. UV photoemission spectroscopy (UPS) has been used to obtain electron energy distributions for the samples under test to extract estimations for the valence band maximum (VBM) and the WF of the surfaces. The lowest WF achieved was estimated at $1.79eV$. Simulated solar heating of the samples by an IR laser, employing the use of a diamond-like-carbon (DLC) absorber surface, was used to measure emission currents from the sample. Emission currents were obtained for the main samples under test as well as for the common NEA-imparting hydrogen termination as a comparison for the other samples due to the well-documented properties it bestows. The largest emission current achieved for an oxygenated-lithiated surface was $0.016mA$ at $700°C$, although this value was lower than expected, emission was very stable over all six cycles. This work demonstrates the great potential of lithium-oxide nitrogen-doped diamond emitters.

Acknowledgments

I would first like to thank my wonderful supervisor Prof Neil Fox for the opportunity to undertake this project and for his constant support and guidance throughout. I must include a huge mention for Dr Ramiz Zulkharnay and Jude Laverock for responding to my barrage of questions with unending knowledge and kindness, without whom this project would not have been possible. Thank you to my fellow budgies for the company and the venting sessions, especially to Catherine for her friendship and for housing me during a final push for data. Finally, I would like to thank my family and partner, Felix for their love and emotional support throughout my whole education, I wouldn't have been able to do it without them.

Author's Declaration

I declare that the work in this dissertation was carried out in accordance with the requirements of the *University's Regulations and Code of Practice for Research Degree Programmes* and that it has not been submitted for any other academic award. Except where indicated by specific reference in the text, the work is the candidate's own work. Work done in collaboration with, or with the assistance of, others, is indicated as such. Any views expressed in the dissertation are those of the author.

SIGNED: ..... DATE: .....

Contents

1 Introduction

The thermal and structural resistance of diamond serves as a strong basis for the material's use in various industrial settings. Diamond has an exceptionally low coefficient of thermal expansion so opposes change in high-temperature environments. The material's high thermal conductivity coupled with its insulating-to-semiconducting property support its use in applications ranging from high power switching electronics[5] to voltaic micropower batteries[6] as well as thermionics for heat-to-electric power conversion.[7,8,8] A material's ability to resist physical and radioactive degradation[9] through many abrasive perturbations, whilst maintaining its original form ensures its suitability for high-temperature processes and its survival in highly radioactive environments. Thus, diamond is the best candidate for the fabrication and characterisation of thermionic diodes utilising solar or radioactive heat sources.

To produce a highly emissive thermionic emitter, an optimum NEA needs to be achieved and the material must be supplied with sufficient charge carriers (electrons). Doping the bulk of the diamond during CVD growth allows for the donation of electrons. Terminating the surface with sub-monolayer coverage of elements that generate strong surface dipoles, such as alkali metals, provides an electrostatic potential at the metal-semiconductor interface that induces downward band bending. The mechanism of this will be explained in more detail in Section1.1.iii. This project aims to investigate the thermionic properties of diamond as a result of nitrogen doping as well as oxygen and lithium terminations. Various nitrogen concentrations and thicknesses of deposited lithium layers will be investigated. Diamond films will be fabricated using the method of CVD. Oxygen layers will be deposited on the surface of the diamond using UVO-cleaning. Lithium depositions will be conducted in an ultra-high vacuum system by thermal evaporation.

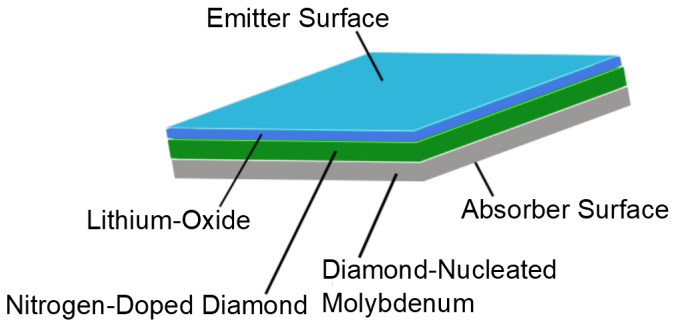

Figure 1: Pictoral representation of a fully-functionalised sample to demonstrate the nomenclature of its components. Relative thicknesses of the different layers are not representative of actual thicknesses, the colours of each layer are also purely for visual clarity and do not physically represent the sample.

Throughout this report, I will explain the advantages of using diamond as an emitter material and the importance of thermionic energy converters, as well as the significance of low-work function functionalisation in the wider field of physical chemistry. The reasoning behind the chosen functionalisations will be explained in relation to previous work conducted by those in the field, and also by a description of the electronic and physical properties and changes of the material at each stage of fabrication.

Nitrogen is a common dopant when it comes to diamond synthesis[10,11,12,13,14,15,16,17,18,19,2021,22,23,24,25,,26] due to its easy incorporation into the diamond lattice. Although the element is a deep-level donor, it does act as an electron source to the fabricated diamond film, something which is crucial for the use of diamond semiconductors in electronics.

Lithium has been tested as a potential terminating species due to its status as an alkali metal allowing it to induce an NEA through interactions on the surface of the material. It has been tested both experimentally and theoretically and has exhibited reductions in the electron affinity (EA) and WF of a material.[27,28,1,2,3]

Oxygenation has been investigated as a terminating species[2] and has also been shown to both increase the adsorption energy (E_A) of the lithiated surface[27,28] as well as to further decrease the EA.[284,2]

Other dopants and terminants have been investigated by others to produce materials with large NEA and low WF to produce optimal emission currents. A few of these species are described in the tables below.

Species	Substrate	Orientation	Concentration $/cm^{-3}$	ϕ $/eV$	J_{1500K} $/Acm^{-2}$	Reference
N	Mo	UNCD	10^{21}	1.29	88	29
N	Mo	UNCD	-	1.42	26	30
N	Mo	Polycrystalline	-	2.22	0.47	31
N	Mo	Polycrystalline	4×10^{19}	1.5 – 1.9	0.093 – 210	32
N	Diamond	(100)	3.3×10^{19}	2.88	0.032	33
N	Diamond	(100)	4×10^{19}	2.4	-	34
P	Mo	Polycrystalline	5×1020	2.3	0.63	35
P	Diamond	(100)	10^{17}	0.67	0.0029	33
P	Diamond	(111)	4.4×10^{18}	1.45	0.33	33

Table 1: Work function and calculated emission current values for nitrogen and phosphorus-doped diamond, terminated with hydrogen. UNCD is ultra-nanocrystalline diamond, *phi* is the work function and J_{1500K} is the emission current calculated at 1500K.[8] Dashes are used where certain values are unknown from the reference data.

Species	Orientation	Coverage /ML	E_{ad} /eV	EA /eV	Reference
Li	(100)	1	−3.26	−2.70	1
Li	(111)	1	−1.50	−0.81	36
Ni	(100)	0.25	−4.25	−0.29	37
Cu	(100)	1	−2.93	−0.55	37
Al	(100)	1	−4.11	−1.47	38
H	(100)	1	−4.14 – −5.36	−1.94 – −2.2	39,40,41,1,38,42
H	(111)	1	−4.37	−1.98	28

Table 2: The following table gives the theoretical adsorption energies (E_{ad}) and electron affinities (EA) of various species terminated on the bare (un-doped) diamond.[8]

Species	Orientation	Coverage /ML	E_{ad} /eV	EA /eV	Reference
Li	(100)	1	−3.64	−3.5	36
Li	(111)	0.5	−4.37	−3.97	43
Na	(100)	0.5	−2.41	−1.30	36
Cs	(100)	0.25	−2.19	−2.41	36
Mg	(100)	0.5	−3.92	−2.77	36
MgO	(111)	0.25	−5.72	−3.08	44
Al	(111)	0.25	−7.31	−2.17	45
Cu	(100)	0.5	−2.35	−1.28	46
Zn	(100)	0.5	−1.13	−3.05	46

Table 3: Theoretical adsorption energies and electron affinities of metal terminants on oxygen-terminated, undoped diamond. For the larger atomic species, such as Al, NEA values depend on which surface bonding structure has arisen from the termination, the lowest NEA has been represented in this table.[8]

1.1 Diamond as a Semiconductor

1.1.i Diamond Properties

Diamond has many advantageous properties that make it suitable for applications where a physically and thermally robust material is needed. Due to its thermal conductivity and expansion coefficient, its capabilities are unaffected by high-temperature environments. The materials physical robustness means its use in industrial applications reduces the risk of device damage as well as the need for constant repair and maintenance.
Highlighted below are the main properties of this wonder material compared to that of its most common substitutes.

Material	Electrical Conductivity /Sm^{-1}	Thermal Conductivity /$W(mK)^{-1}$	Thermal Expansion Coefficient /K^{-1}	Band Gap /eV
CVD Diamond	(Resistivity of $10^{12} - 10^{16} m$)[47]	2100 (at $298K$)[47]	1×10^{-6} [48]	5.45[47]
Natural Diamond	(Resistivity of 10^{18})[47]	2000 – 4000 (at $80K$)[47]	$1.5 - 4.8 \times 10^{-6}$ (at $400 - 1200K$)[47]	5.45[47]
Graphene	80×10^{6} [49]	4000[50]	-8×10^{-6} [49]	0[51]
Silicon	(Resistivity of $2.3 \times 10^{3} m$)[52]	148[53]	2.6×10^{-6} [54]	1.12[55]
Molybdenum	1.9×10^{7} [56]	138[57]	4.8×10^{-6} [57]	0

Table 4: Physical and electrical properties of diamond along with that of its common competitors in the electrical industry. Silicon and molybdenum are used in the CVD industry and process due to their reasonably similar thermal expansion coefficients. Where Sm^{-1} is Siemens per meter, $W(mK)^{-1}$ is watts per meter kelvin, K^{-1} is per kelvin and eV is electron volts.

1.1.ii Physical and Electronic Structure

Carbon is a group four element so forms tetrahedral bonds. Diamond carbon is comprised of a five-atom unit cell where the carbon atoms are bonded through four sigma bonds, the strongest form of covalent bonding due to head-on overlapping of the electron orbital clouds.[58]

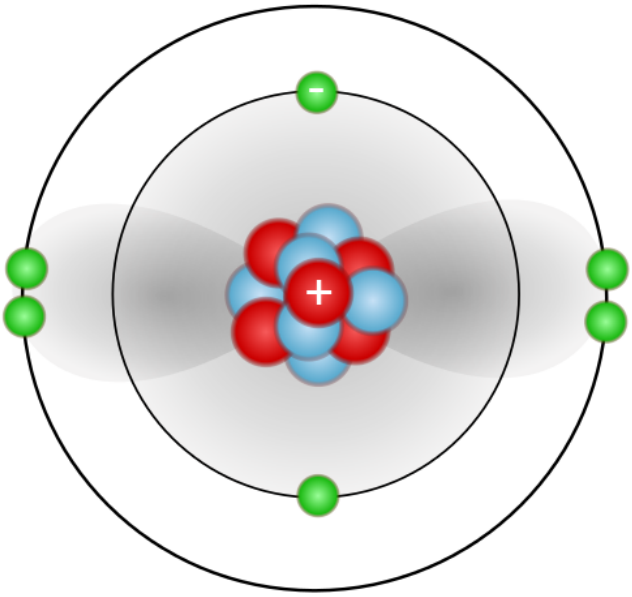

Figure 2: Atomic structure of carbon showing six protons (red), six neutrons (blue) and six electrons (green). The p and s orbitals are shown in grey.

Hybridization of the valence s and p orbitals results in four identical sp^3 orbitals, each containing a single electron with spin orientated away from the nucleus, towards the donor carbon atom, forming covalent sigma bonds. Hybridization of the involved orbitals leads to the greater directionality of the sigma bonds which leads to greater orbital overlap, thus the formed bonds are stronger than non-hybridized carbon bonds.[58]

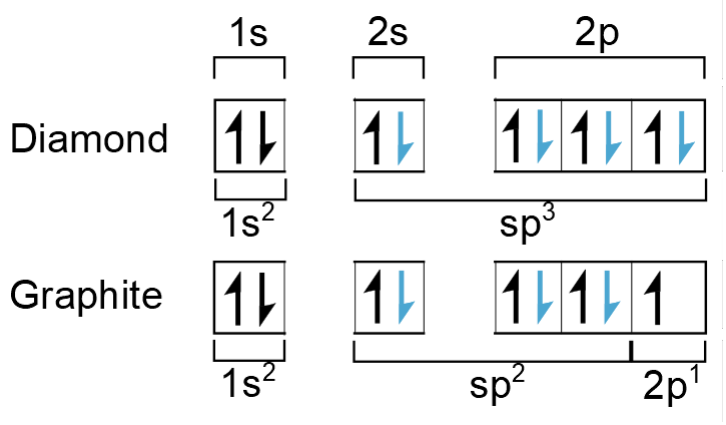

Figure 3: Carbon electron shells hybridize in different ways to form either the diamond or graphite structure, leading to the unique properties of both. sp^3 orbitals produce a diamond structure and sp^2 orbitals produce a graphite structure. The electron structure for each of these materials is shown above.

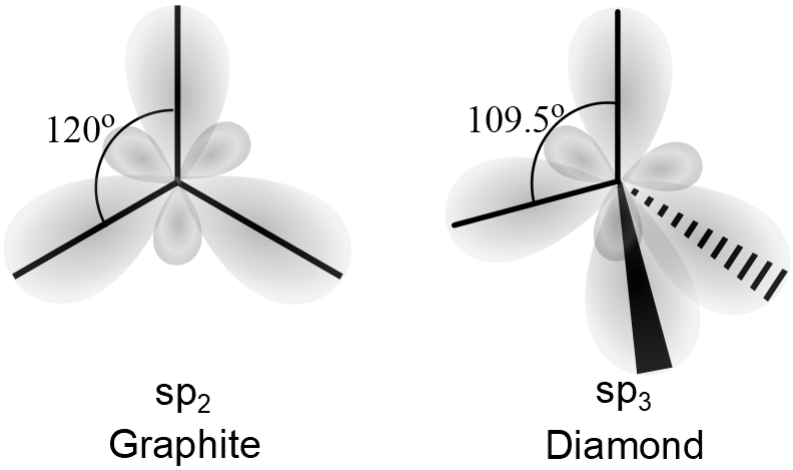

Figure 4: Orbital structure and orientation of carbon bonding as a result of the various carbon hybridizations are shown in the above diagrams. That on the left shows the resulting structure and trigonal planar shape of graphite, on the right shows the resulting tetrahedral shape of diamond.

Allotropes are different forms of a pure element as a result of varying bonding structures. For carbon, materials produced by different atomic configurations vary from diamond to graphite to coal, arising in their famously contrasting properties.
In the case of graphite, four carbon atoms are bonded together with two sigma bonds and

one pi bond. Electrons in the pi pond are delocalised, this gives graphite its fantastic conductive ability. Hybridization also occurs in graphite, but two valence p orbitals hybridize with the valence s orbital to form three identical sp^2 orbitals, unlike the four sp^3 orbitals formed in diamond. The three sp^2 orbitals form sigma bonds with three respective carbon atoms. The remaining p orbital is orientated perpendicularly to these sp^2 orbitals and so can adjacently overlap with the other p orbitals to form a pi bond.[59]

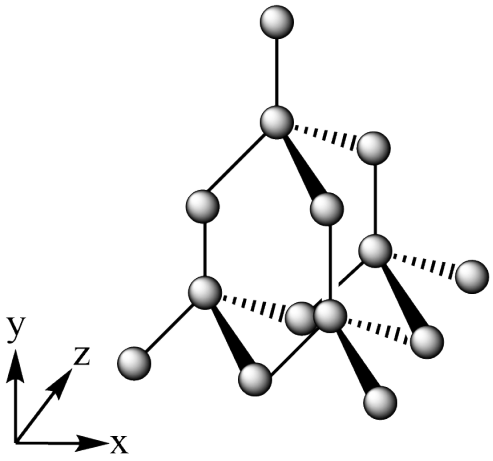

Figure 5: Here shows the physical and bonding arrangement of the giant covalent structure, diamond.

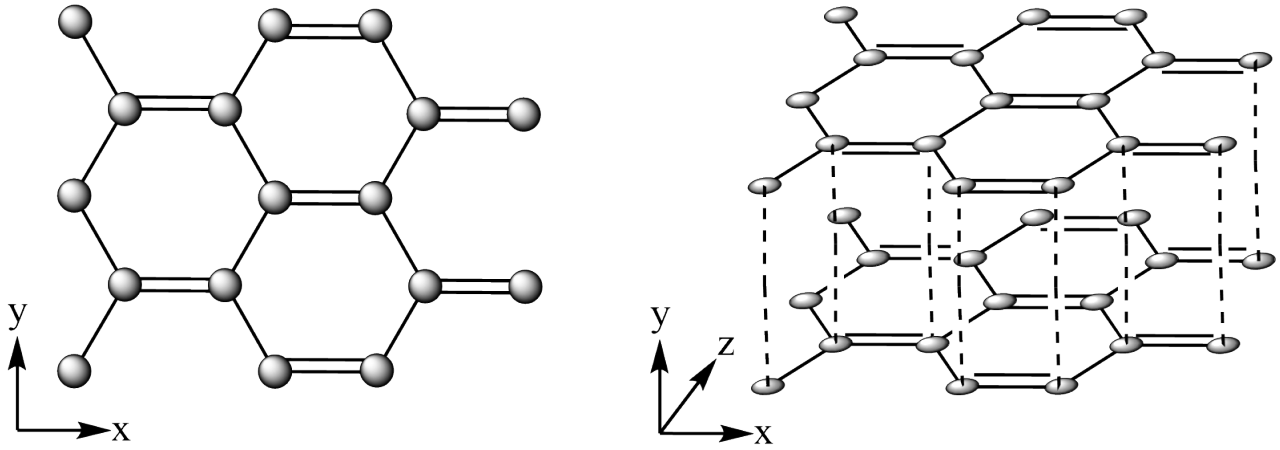

Figure 6: Here shows the physical and bonding arrangement of graphite. The strong covalent bonds between carbon atoms are shown as solid lines, and the weak bonds between layers as a result of Van der Waals interactions are shown as dashed lines.

1.1.iii Band Structure

Fermi energy is the highest energy an electron can have at $0K$.[60] Electrons are ordered into sequential states starting from the lowest possible energy up to the Fermi energy. No

electron can surpass the Fermi energy unless externally excited, hence why the Fermi energy could be considered as the electron chemical potential.
The Fermi level is the energy level where the probability of electron population is 50% at any temperature. Hence, why at higher temperatures, the Fermi level increases in energy, because more electrons have higher energies. Fermi temperature is the temperature at which the Fermi level is equal to the Fermi energy.[60]
The Fermi level lies between the valence and conduction band, as statistically half of the electrons should exist at that energy. At $0K$, no electrons can have greater energy than the Fermi level. The Fermi level exists as a result of the Pauli exclusion principle, no two leptons (like electrons) can have identical quantum numbers/energy states, this is what has led to the concept of shells and orbitals. So if a system has more than one lepton, each lepton will have a different set of magnetic quantum numbers (QN) associated with it.[60]
Magnetic QN define the orientation of the orbital depending on its energy and shape. This differentiation splits sub-shells into individual orbitals, placing one electron in each. Consequently, the magnetic QN determines the total number and orientation of each sub-shell. As each electron has a different magnetic QN, they each have a different combination of orbital occupation and orientation (spin) and thus have different energies.[61]

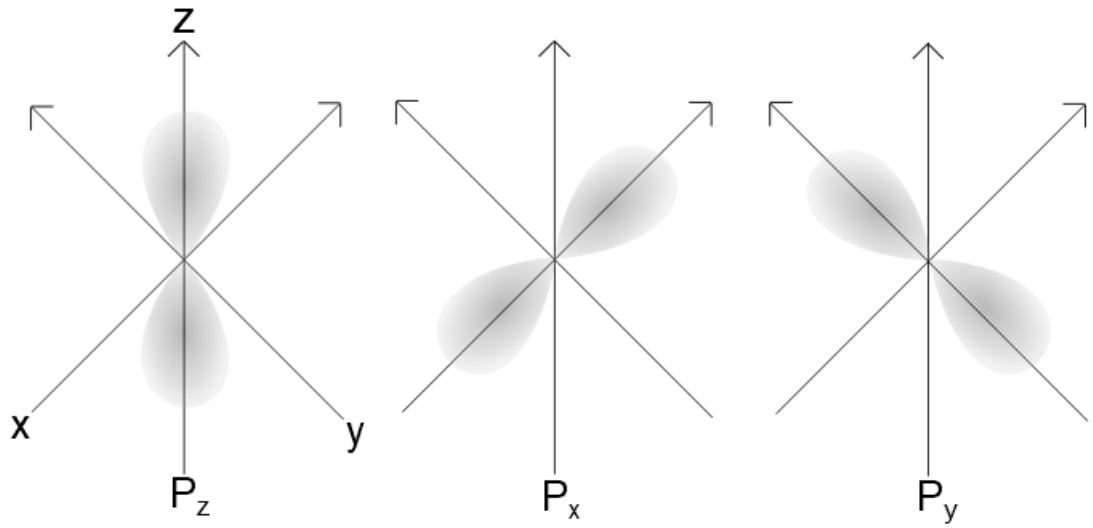

Figure 7: The orientation of the p orbitals changes with the quantum number. P_z aligned orbitals have a magnetic QN, m_1=0. P_x and P_y give QN of m_1=±1.

Energy states available to electrons are not discrete but instead form bands of possible energy values.

Conduction occurs when electrons are in the conduction band (CB) as it is directly adjacent to the valence band (VB), in this state electrons have zero potential energy and positive kinetic energy. Insulation occurs when electrons are in the VB, below the CB, and the gap between the two bands is large. In the VB, an electron has negative potential energy and

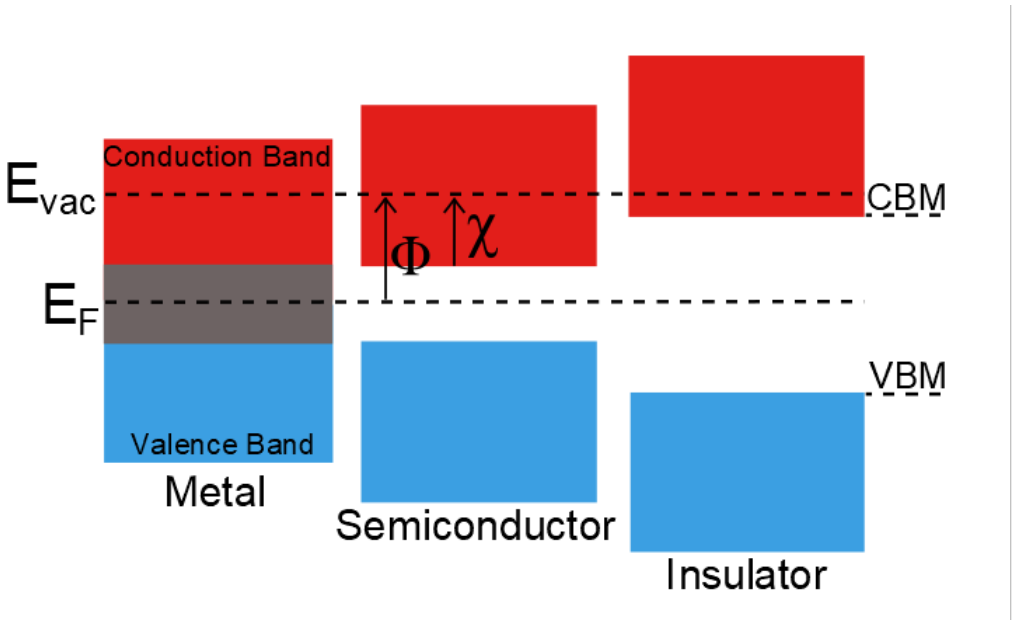

Figure 8: Electronic band structure for different material types. E_F is the Fermi energy level, and E_{vac} is the vacuum energy level at which electrons have escaped the material. Φ shows the material's WF as the energy needed to excite an electron from the Fermi level to the vacuum level. χ shows the EA, the difference in energy from the conduction band minimum (CBM) to the vacuum level, in this diagram, it has a positive value (PEA). VBM denotes the valence band maximum.

zero kinetic energy. If the maximum of the VB (VBM) and the minimum of the CB (CBM) lie at different energy values, the band gap is indirect (semiconductors), if they lie at the same energy level the band gap is direct (conductors).

Semiconductors may have a small enough band gap that thermal or other excitations are enough to promote electrons from the valence band.[62] Semiconductors like diamond have large band gaps that allow for the manipulation of the Fermi level, thus the work function. For intrinsic semiconductors, the Fermi level is essentially halfway between the CBM and VBM, so no conduction occurs at $0K$.[63]

Diamond is one of a few special materials that have a wide band gap structure (such as AlGaN[64] and cubic boron nitride[65]), and electron energies such that the CBM lies above the VBM. This results in an NEA and can be described as a 'true' NEA. A few other materials have been found to also possess a true NEA, including AlN,[66] GaAs, InP and Si.[67]

Donors and acceptors can be doped into diamond material in the growth phase to manipulate the electronic structure, by donating or accepting electrons respectively. In semiconductor electronics, shallow donors are the most desirable, these donors provide additional energy levels within the semiconductor band structure closer to the CBM. Deep donors provide the reverse, electron energy levels deeper in the band structure of the material closer to the VBM.

WFs of semiconductor materials can be adjusted due to the phenomenon of band bending, the manipulation of the electronic bands within a material. An NEA can be produced, allowing electrons to be liberated from a material through thermionic processes.

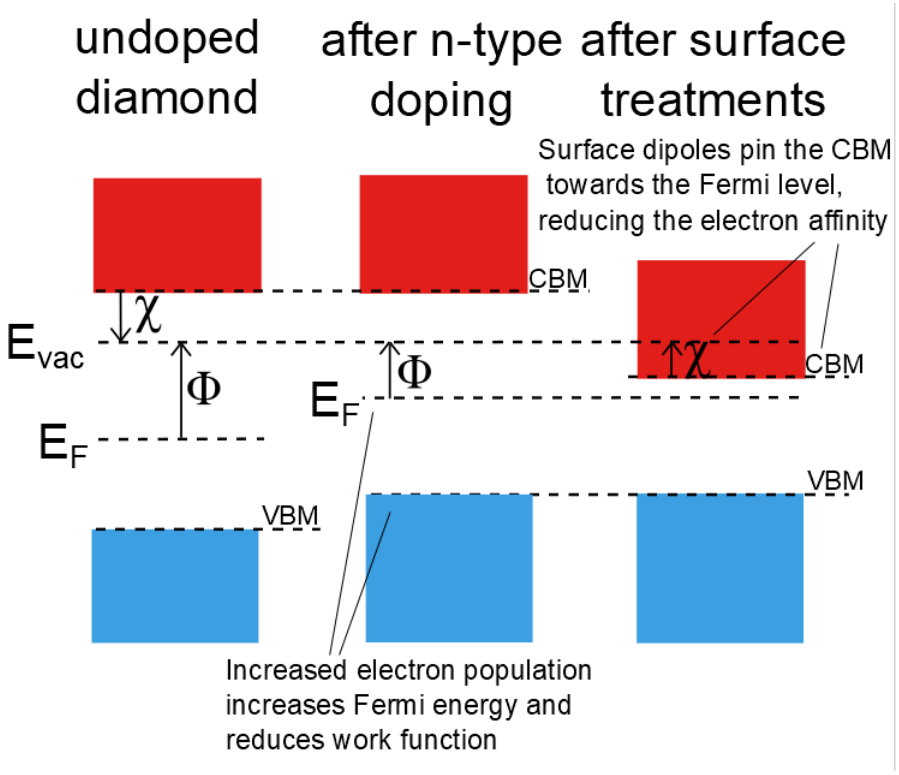

Figure 9: Shown here is the band structure of the material as bare diamond, n-type doped diamond and n-type doped diamond with surface treatments. After n-type doping the electron population is increased which increases both the VBM and the vacuum level, this reduces the work function. After surface treatments, surface dipoles are created which induce downward bending of the CBM towards the Fermi level. The combination of reduced work function and decreased electron affinity theoretically produces an effective thermionically emitting surface.

The process of band bending was first conceptualised by Schottky and Mott to explain metal-semiconductor contact interfaces. Band bending is the shifting of the Fermi level within a material, it is a direct result of a difference in WF between two materials in contact.
When a metal and semiconductor are in contact, an electron potential is created across the interface. Electrons move from the material with the lowest WF (metal surface terminant) to that with the highest (diamond semiconductor), because the electrons can reduce their energy by moving from the metal to the conduction band in the semiconductor. Transfer of electrons continues until the Fermi levels of the two materials have reached equilibrium. In other words, the chemical potential of the semiconductor reaches equilibrium with the Fermi energy of the metal. It's this energy difference between the electrons in the two materials that drives this movement, once these energies are equal, the movement stops. A

slight negative charging of the semiconductor due to its newly accepted electrons inhibits the further flow of electrons into the CB. In this region of the semiconductor at the interface electrons, and so a negative charge, have accumulated. This is named the accumulation layer. This region acts like a potential barrier that causes deformation of the energy bands in the semiconductor close to the interface. The chemical potential of the semiconductor in this region has increased due to the acceptance of higher energy electrons from the metal. This potential is pinned at the interface, the position of which moves to be in equilibrium with the metal after transport. The structure of the bands in the bulk of the material is unaffected apart from the uniform downshift in energy. The bands in the metal do not shift, nor is the Fermi level noticeably affected due to the large number of valence electrons in the metal compared to that of the semiconductor, where most of the electrons are donated by dopants.[8,68,69,70]

The WF of a material is the energy required to liberate an electron from the Fermi level to the CB.[8] The energy of the electron as it leaves the surface of the material is the difference between the incident energy and the WF, this is described by the photoelectric effect.

$$E_{photon} = \phi + KE_{max} \tag{1}$$

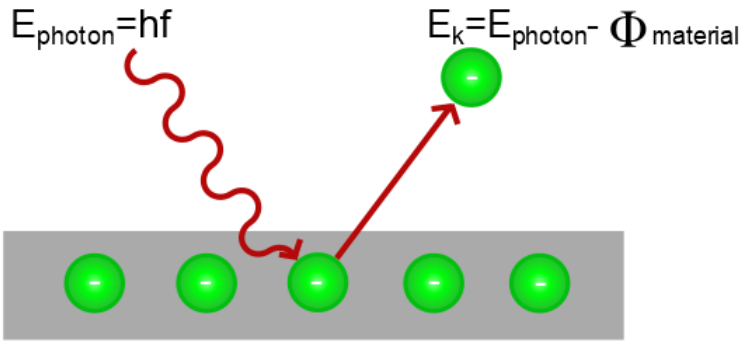

Figure 10: Here shows the process of incident photons interacting with electrons on a singular basis, if the energy of the photon (frequency) is greater than the binding energy (work function) of the material then the electron will be ejected from the surface of the material. If the energy of the photon is greater than the work function of the material, the electron will leave the surface with some kinetic energy. Photons are shown as a wave in this diagram, however, this theory led the way in wave-particle duality.

The ionisation energy is the energy required for an isolated, gaseous atom in the ground state to discharge an electron. Each successive electron requires more energy to be expelled due to the increasing electrostatic forces as the distance from the positively charged nucleus

decreases. Hence it is a function of atomic radius. This increase in required energy is also a result of the increase in positivity of the atom's overall charge as each electron is lost. The more shells an atom has, the less attraction outer electrons feel to the nucleus due to the negative charges of inner shells partially cancelling out the positive charge of the nucleus. This shielding effect lowers the ionisation energy.[71]

EA is the energy released when gaseous atoms acquire an electron. It is the measure of attraction between the incoming electron and the nucleus. The stronger the attraction (greater the difference in charge) the more energy that is released. EA decreases as the number of inner shells and atomic radius increases. As the number of shells increases, the shielding effect reduces the attraction between incoming electrons and the nucleus hence less energy is released. The same is true for the effect of an increased atomic radius.[72]

In N-type semiconductors, the dopant is a donor impurity and contributes free electrons, hence electron energy levels, increasing the energy of the Fermi level, thus raising it towards the CB. Electrons can then be easily excited to the CB. In p-type semiconductors, the dopant is an acceptor impurity and creates a hole. So, extra hole energy levels reduce the Fermi level, lowering it towards the VB. The extra holes in the band gap allow the excitation of VB electrons, leaving mobile holes.[73]

1.2 Diamond Thermionic Device

1.2.i Introduction

Thermionic emission can be characterised by the Richardson-Dushman equation[74] :

$$J(T) = A_R T^2 exp\left(\frac{\phi}{kT}\right) \tag{2}$$

Here, $J(T)$ is the current density as a function of T, the absolute temperature, A_R is the Richardson constant, ϕ is the WF of the material and k is the Boltzmann constant. The Richardson constant, A_R must be corrected by an experimentally-determined factor as it assumes uniform WF and temperature across the whole sample which, especially for functionalised diamond films, isn't always the case. However, the model still gives reasonable predictions for the emission current.[8]

TECs incorporate an emitter (cathode) and a collector (anode) surface. Upon thermal irradiation to the absorber surface of the emitter material, electrons are liberated and travel through a vacuum, producing a self-bias, before being captured by the collector surface. Electrons in the collector increase the Fermi level, increasing the potential across the surfaces as well as the current in the external circuit. The WF of the collector must be lower than that of the emitter to be able to collect emitted electrons. This difference in WF also allows for the mitigation of reverse currents. A small gap between the two surfaces is required to minimise the operating potential such that the barrier height for electrons in the collector

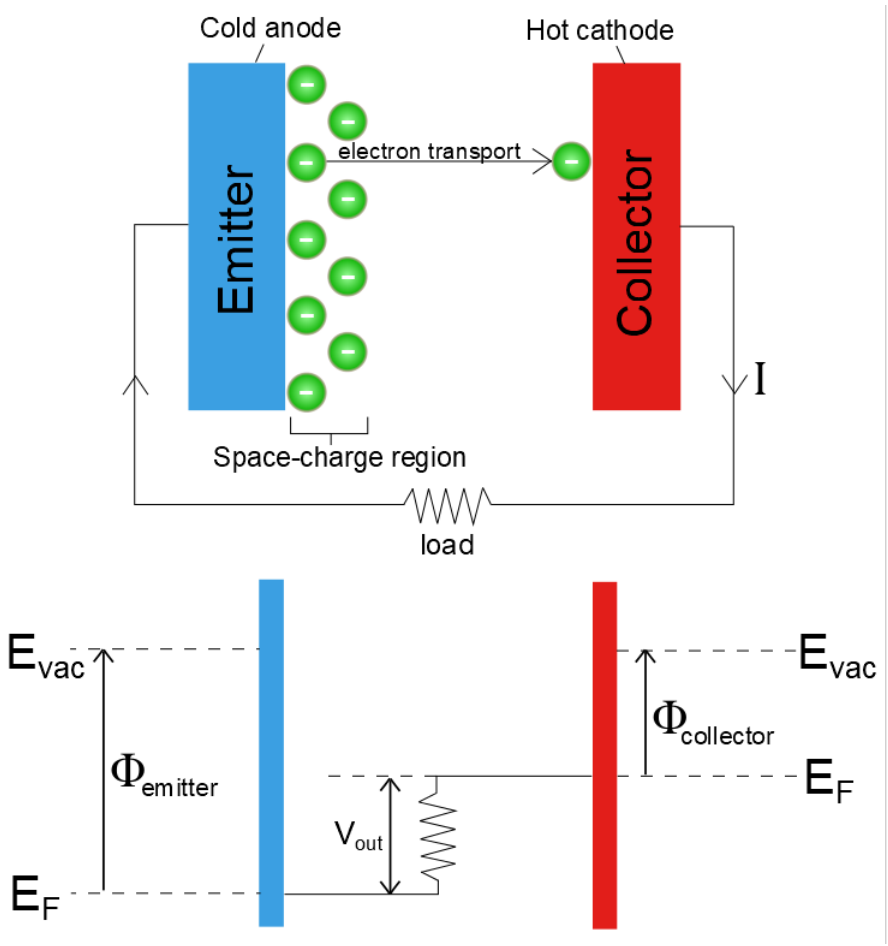

Figure 11: The top diagram shows a basic schematic of a thermionic energy converter comprising of emitter and collector electrodes. A bias is applied to replenish the electron population in the emitter for continuous electron emission, the produced electron current drives an electrical load. A temperature gradient between the two plates drives this transport due to the difference in energies. The lower diagram shows the difference in Fermi levels of the two materials as a result of the electron transport, where this difference, also equal to the difference in work functions, gives the maximum voltage output.

isn't increased.

TEC devices usually work under vacuum to both increase the mean free path of the electrons and to ensure the electrodes are not in thermal contact. In theory, TEC devices are efficient, they can be modelled as simple engines so their efficiencies can be predicted by the Carnot equation, they are also long-lasting as they have no moving parts, however, they do pose physical challenges in their development and fabrication. Other than the obvious engineering challenges of building a device consisting of two electrodes in close proximity whilst remaining thermally isolated, space charge effects also must be addressed to produce a high-functioning TEC. Space charge is the accumulation of electrons within the vacuum region, these electrons don't have the required kinetic energy to travel through the vacuum gap to the collector, they travel back to the surface of the emitter, forming a cathode cloud

which hinders further electron emission due to the produced potential barrier.[8]
High operating temperatures ($> 1000°C$) are often needed for TEC devices due to low emission efficiencies as a result of space charge effects and heat transfer between the two electrodes. Increasing both the thermal absorbance and emission capabilities of such devices is needed to develop their great potential into highly efficient systems capable of operating at low temperatures, whilst also meeting the energy needs of a vast number of possible commercial and industrial uses.
Thermionic devices are able to utilise not only abundant solar and waste thermal energy for power generation but also radioactive thermal sources for energy conversion in applications in which solar radiation is unavailable. Examples of the potential of a TEC device include lunar exploration and space travel.

1.2.ii Thermionic Devices

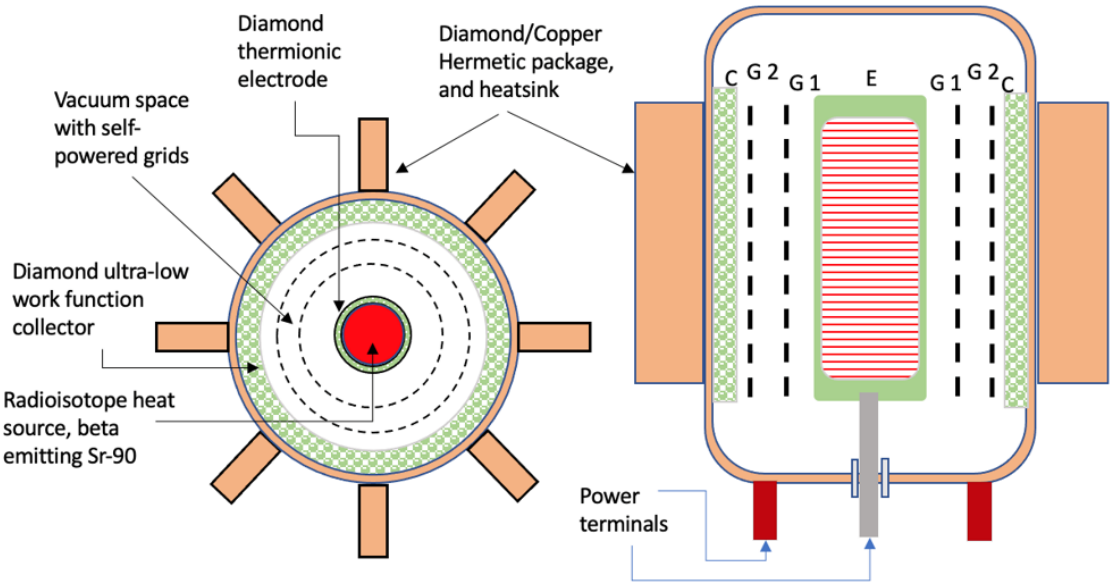

Figure 12: Shown here is a possible design concept of a mature thermionic energy converter using a radioactive heat source for the application of energy generation for space exploration. The image on the right shows the cross-sectional side view of the image on the left. C denotes the collector. G1 and G2 are the self-powered grids and E shows the emitter.

You could ask yourself why such a theoretically simple and attractive device has yet to be available for wide-scale electricity generation, the answer to that question lies within the intricacies of the fabrication of micro-scale structures. Emitter and collector surfaces must have low topographies for efficient transverse and orthogonal electron transport. in the case of diamond films, samples must have low graphitic content to improve the isotropic nature of the atomic structure. Electrodes comprising the converter device must be in close enough

proximity to reduce the distance needed to travel by electrons, both to increase the probability of collection and also to increase the energy of the electrons that have made the journey. However, as these devices are heat engines, the electrodes must exist with a thermal potential across them, with the emitter at a higher temperature than the collector. In practice, keeping two surfaces from being in thermal contact whilst minimising the distance between them is difficult, keeping a vacuum between the two plates is the best way so far to combat this issue.

The two comprising electrodes of a complete thermionic device must have a work function potential across them, the greater this potential, the greater the possible power output of the device. So not only is reducing the work function of the emitter surface important, more so is reducing that of the collector surface.
Space charge mitigation has been under study by various groups as it is one of the biggest obstacles for thermionic technology. Some suggest using gases to neutralise the electron cloud[75] or to absorb electrons and travel to the collector as ions.[76,77,78] The presence of hydrogen in the electrode gap has shown to increase emission current through the mechanism of absorbing the space charge region electrons.[77]

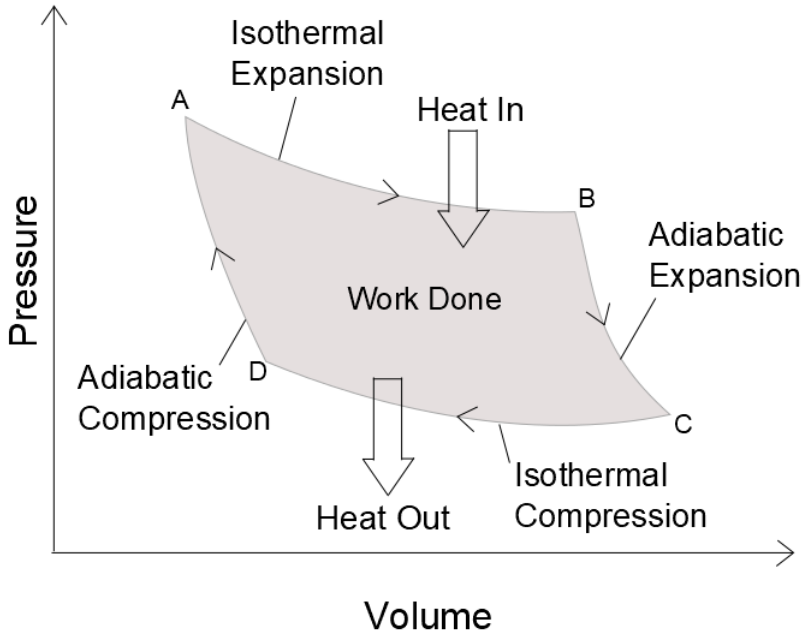

Figure 13: The ideal Carnot heat engine cycle shown in terms of volume and pressure changes of a system. From A to D, the system undergoes isothermal and adiabatic expansion, then isothermal and adiabatic compression. The area enclosed by the curves shaded in grey gives the work done by the system to transfer the heat involved with this process.

As a thermionic converter is a simple heat engine, its efficiency is described by that of a

Carnot cycle:

$$Efficiency = 1 - \frac{T_C}{T_H} = 1 - \frac{|Q_H|}{|Q_C|} = \frac{W_{OUT}}{Q_{IN}} \tag{3}$$

As can be seen by the above equation, the efficiency is limited only by the temperatures of the two electrodes. There are no moving parts in such a device so no frictional or mechanical losses of energy take place. Losses in electrical efficiency of TECs are due to space charge accumulation hindering the continual flow of electrons and any thermal losses of the two plates.[8]

2 Functionalisation of Diamond as an Emitter Surface

2.1 Diamond Synthesis

In this section, the process of diamond synthesis will be discussed and described in detail. Diamond films in this work have been grown on molybdenum substrates ($10x10mm$ squares with a thickness of $0.5mm$). Microwave-assisted CVD (MW-CVD) is used for the synthesis of these films. The mechanism of which and conditions used for growth will be discussed in the coming sections. Bulk doping of the grown diamond material will be implemented to increase the charge carrier density within the film. Nitrogen has been chosen as it is an electron donor and promotes n-type conductivity.
Oxygen treatment of the diamond surface will be used as a precursor to lithium terminations to increase the adsorption energy and bond strength of the adsorbent layers. Hydrogen has also been investigated as a potential alternative to oxygen but, as will be discussed, is not as practically effective as oxygen.
Lithium terminations will be the final stage of emitter surface functionalisation, chosen for the dipoles produced by the species on the surface that redistribute the electron density towards the carbon and oxygen atoms below, inducing the downward bending of the CB towards the VB.[79]
Thicknesses and dopant concentrations of nitrogen-doped diamond (NDD), as well as thicknesses of deposited lithium, will be under investigation for the effects they have on the thermionic properties of the fabricated material.

2.1.i Substrate Nucleation

Substrates require nucleation with a form of diamond nano-particles to seed the surface as preparation for film growth in the CVD process.
All methods involve washing the substrate with either methanol in an ultrasonic bath for $15minutes$ before nucleation can begin. The chosen method in this work is electrostatic nucleation.[80] This process involves mounting the substrates on a disk, using carbon tape as an adhesive, that has its rotation controlled by a motor. The substrate mounting is placed in a perspex box on the face opposing a fixed syringe. The syringe is filled with a mixture of diamond nano-particles ($0.05\mu m$) diluted in $35ml$ of methanol and attached to an external voltage of $65V$. $2ml$ of this diamond-methanol solution is accelerated towards the substrates, due to the electrification of the solution, producing a parabolic path from the syringe to the substrate mounting.

Electrostatic nucleation, also known as electrospray, produces uniform coatings of the diamond seed. Penetration and incorporation of which is not as strong as other nucleation

methods such as manual abrasion.
For increased seed incorporation but a slightly greater risk of CVD diamond film delamination, manual abrasion can be used as a seeding technique. This involves manually abrading the surface with nano-diamond ($1 - 3\mu m$) and a metal tool, to both scratch the surface and embed the diamond particles. Another method tested in this work is ultrasonic nucleation, in which the substrate is placed in a beaker containing the methanol and diamond nanoparticle mixture, and a sonicator is used for $1 hour$ to incorporate the mixture and substrate. This method, although resulted in a uniformly seeded substrate, produced highly delaminating diamond films.

2.1.ii Microwave-Assisted Chemical Vapour Deposition

Parameter	Value
N flow rate	$0.3 sccm$ or $0.5 sccm$
H flow rate	$300 sccm$
CH_3 flow rate	$12.5 sccm$
Temperature	$1000°C$
Pressure	$130 Torr$
Power	$1.3 kW$

Table 5: CVD growth parameters and their values for diamond film growth within this project. All conditions other than nitrogen concentration were kept constant so that the effect of varying nitrogen concentrations could be investigated. Such species content throughout this work is described as concentration although it is important to point out that values given for nitrogen amounts are in terms of gaseous flow rates for the gaseous growth mixture in the CVD process, where sccm represents standard cubic centimetres and gives the flow amount per second.

Seeded substrates are placed in the reaction chamber under vacuum to undergo plasma treatment, a gaseous mixture of molecular hydrogen and methane. Hydrogen is disassociated by the MW radiation to its atomic form, which breaks down the methane molecules to produce methyl radicals, these deposit on the substrate surface at available bonding sites. Atomic hydrogen reacts with a hydrogen atom of the deposited methyl radical, leaving CH_2 on the surface. As it is energetically favourable, the bonds are broken between the carbon and two hydrogen atoms, and only the carbon atom remains. This process continues for the growth period and carbon atoms from the methyl groups build up to form diamond.[11] Atomic hydrogen also etches away at the surface at a lower rate than the production of diamond, this removes any graphitic content from the non-hybridised carbons that may have formed on the surface.

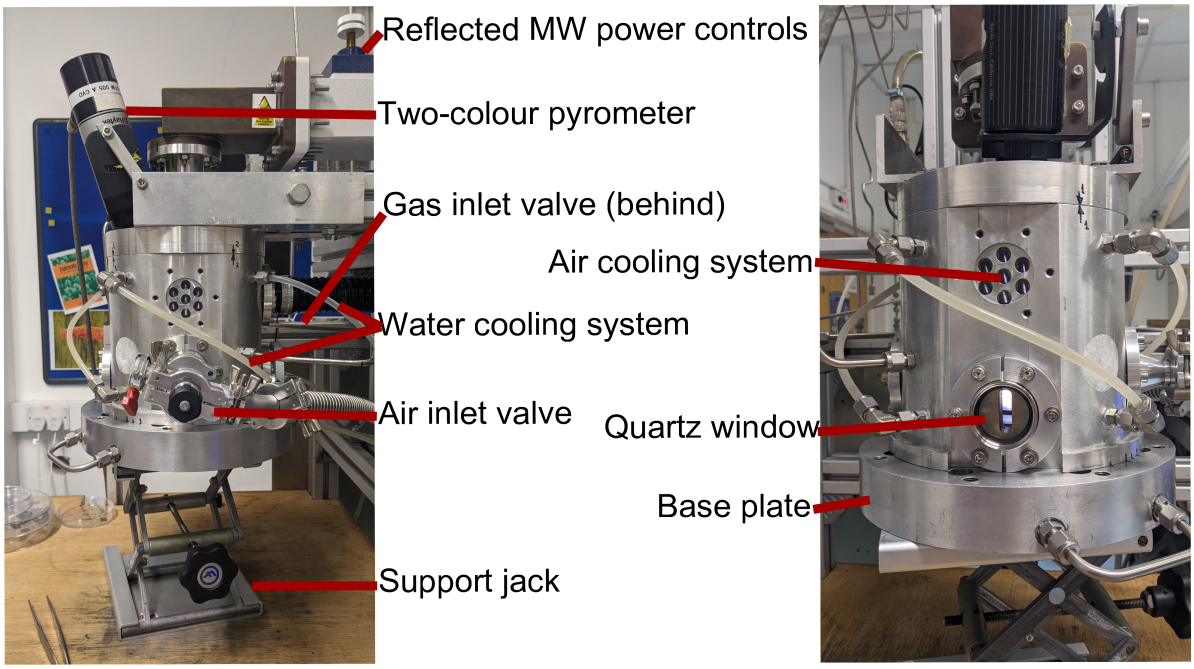

Figure 14: The above diagram shows the front and side views of the CVD chamber, annotated with its various components. The base plate is lowered using the support jack to allow for sample mounting. As its name suggests, the air inlet valve controls air flow between the chamber and the atmosphere to allow vacuum pressure to be reached within the chamber once connected to the vacuum pump.

Temperature is measured using a two-colour pyrometer, which calculates the temperature from the colour of the plasma, dependent on the emissivity of the sample. The temperature seems to fluctuate at the beginning of the growth, this is because the emissivity of the sample changes, from that of the substrate to that of CVD diamond. A two-colour pyrometer is needed for improved accuracy due to the variation of plasma colour depending on the constituent dopants; Hydrogen produces a purple plasma, but once methane is added, the plasma turns more yellow. The emissivity given to the pyrometer is that of the substrate ($\epsilon_{Mo} = 0/18$) as the emissivity given doesn't continually match that of the diamond growth sample as a whole, the temperature displayed can't be taken as an exact value but provides a reasonably accurate estimate. High temperatures ($1000 - 1400^{\circ}C$) are needed for the structural reconstruction of graphitic carbon into diamond. Resulting diamond orientations are determined by the growth temperature, lower temperatures coupled with low chamber pressures give a triangular (111) orientation. Increased temperatures and methane concentrations give square and rectangular (100) crystals, however increasing these parameters above certain amounts ($1400^{\circ}C$ and $\geq 0.5sccm$) destroys this morphology and leads to a larger graphitic content.[81,22,12] polycrystalline films exhibit multiple orientations, samples produced in this work will be polycrystalline as a result of their dopants and substrates. Microcrystalline films exhibit small grain sizes and are obtained from low methane

concentrations and temperatures. Nanocrystalline films are produced at higher methane incorporations. The film is smoother than that of microcrystalline films but has less extreme mechanical and electrical properties.[81]
Molybdenum substrates have not only been chosen due to their non-melting nature and minimal thermal expansion at the diamond growth temperatures but also due to the possibility of carbide layer formation on these nucleated substrates. Mo has a reasonable solubility with carbon so only forms this carbide layer at the surface interface. Substrates that readily react with carbon, more so than species similar to molybdenum, impede diamond formation due to their high solubility with respect to carbon, so understandably would affect the specific structural formation that must take place to synthesise diamond. Carbide layers grown onto the substrate promote diamond growth and increase the structural 'strength' of the sample by somewhat relieving stress at the substrate-diamond film interface. Such layers reduce the potential of diamond delamination, increasing the chance of producing a stable, uniform emission surface.[81]
To produce a carbide layer, the sample is left in a methane-rich environment in the presence of a hydrogen-activated plasma for 5-15 minutes out of the total growth time before dopant gases are added to the mixture.
Molybdenum substrates are also easily fabricated to form an absorber surface, either by laser etching or by the creation of a black-body absorber.
High-quality diamond films are needed for the application of a thermionic emitter, for the electron emission process, smooth surface morphologies are needed to provide emitted electrons with the easiest physical pathway. The physical structure of the crystal also affects the electrostatic interactions between particles which additionally affects the energetic pathway of the electrons. Therefore, smooth surfaces are needed to allow for the easiest form of electron transport as well as to reduce refraction of the electrons across a largely topographical surface, both of which effects would reduce the resulting emission current.

2.1.iii Doping

As previously mentioned, nitrogen is the dopant of choice for the samples fabricated in this work. Nitrogen is a fairly common n-type dopant as it promotes n-type conductivity. It's similar size to carbon allows for substitutional incorporation into the lattice,[20] meaning one carbon atom in the crystal lattice is replaced with one nitrogen atom. The resulting structure has little effect on the diamond structural properties but will affect the carrier concentration.
Nitrogen is however a deep-level donor, the donated electrons add energy levels in the diamond band gap closer to the VBM than the CBM. Hence, shallow donors where the additional energy levels are closer to the CBM offer a more energetically favourable pathway

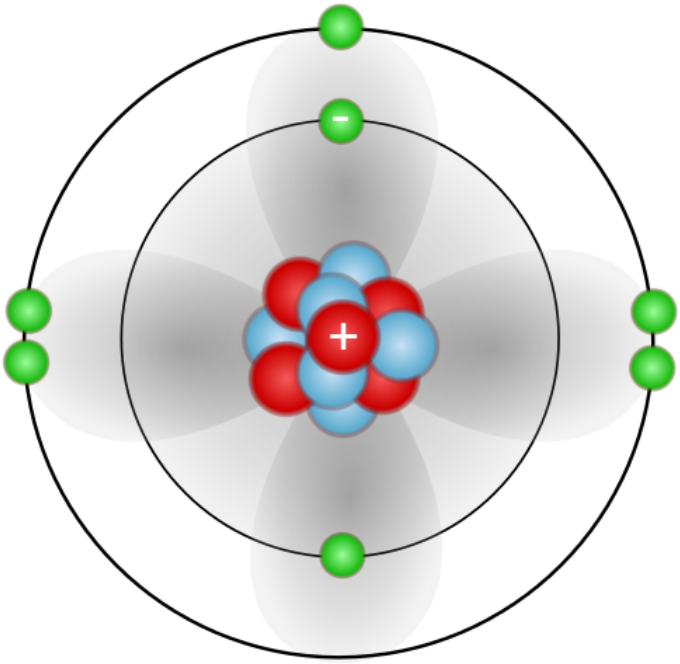

Figure 15: Atomic structure of nitrogen showing seven protons (red), seven neutrons (blue) and seven electrons (green). The p and s orbitals are shown in grey.

for electron transport in the thermionic emission process. To negate the adverse electronic effects of the lower energy donor level, species can be terminated on the semiconductor surface to induce the downward bending of the CBM towards this deep donor level, the process of which is to be described in the next section.

2.2 Surface Termination

2.2.i Terminants

Species more electronegative than carbon can induce band bending at the semiconductor surface. Lithium is a proposed shallow donor if used as a dopant[16] but has been used as a surface terminant due to the surface dipole it creates with the diamond film.

Oxygenation is used to increase the bond strength between the terminated surface layer and the underlying diamond. This increases the stability of the highly reactive lithium layer in air. The addition of oxygen also increases the polarity of the surface dipoles thus further decreasing the work function as desired as a result of increased downwards band-bending. Hydrogen termination has also been shown to reduce the work function but suffers significant desorption at elevated temperatures above red heat, making it problematic for use in high-temperature applications.[82]

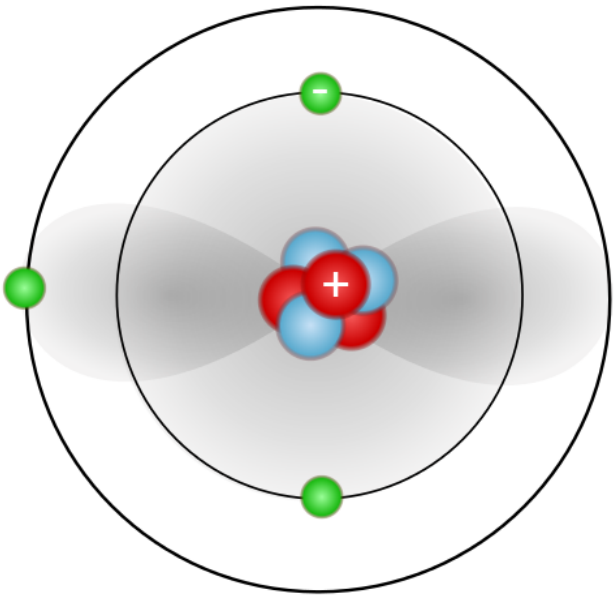

Figure 16: Atomic structure of lithium showing three protons (red), four neutrons (blue) and three electrons (green). The p and s orbitals are shown in grey.

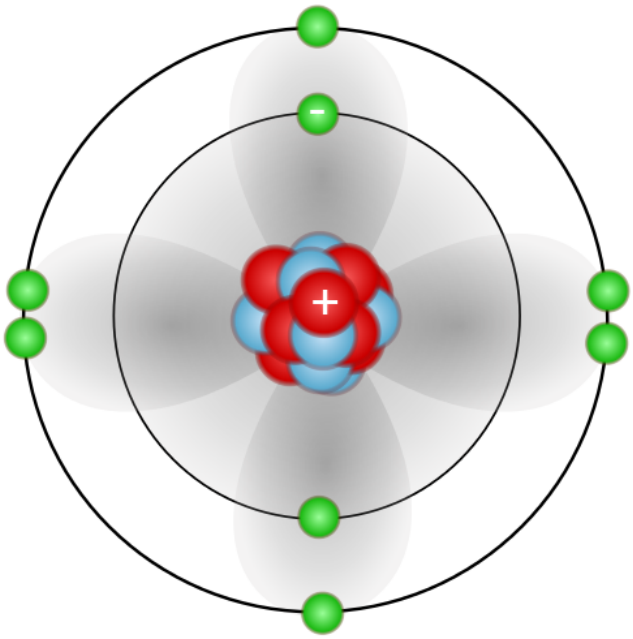

Figure 17: Atomic structure of oxygen showing eight protons (red), eight neutrons (blue) and eight electrons (green). The p and s orbitals are shown in grey.

2.2.ii Surface Bonding

Annealing is used before and after deposition to clean and stabilise the surface respectively. Cleaning the sample involves reaching temperatures of $300°C$ for $1 hour$ at which point, most weakly-bonded contaminating surface species out-gas from the surface. After

deposition, annealing to a higher temperature of $500^{\circ}C$ for $1hour$ also, motivates surface reconstruction to ensure bonding between the new and existing top layer of the surface under study.
Surface energy is the amount of excess energy at the surface of a material compared to the bulk. It increases with both the strength of the interactions and the surface area of the exposed surface. To minimise this surface energy, a material with lower energy can be absorbed onto the surface. Through this process, the number of exposed surface atoms with high surface energy is minimised and replaced with lower-energy atoms.[83] Adsorption is the accumulation of a gas or liquid species on the surface of a solid or liquid substance, forming a film of molecules or atoms. In the bulk of the material, interactions between atoms are isotropic, however, surface atoms or molecules are not completely surrounded by other atoms and so can interact with adsorbents.[84] The absorption energy is the decrease in energy while an adsorbate combines with a surface.[85]
The greater the adsorption energy, the lower the energy of the surface has become, hence the more stable. Thus, the chosen terminants and the amounts deposited must result in large adsorption energy if the surface is to be stable in ambient conditions, a requirement necessary for the practical use of a complete thermionic device.

2.2.iii UV-Ozone Treatment

The primary method of oxygenation in this work is by the use of a UVO-cleaner, where the sample is placed inside the chamber at room temperature and pressure (RTP), and atmospheric oxygen is radicalised by a mercury lamp above the sample.

$$O_2 + hv \rightarrow 2O^{\bullet} \tag{4}$$

$$O_2 + O^{\bullet} \rightarrow O_3 \tag{5}$$

$$O_3 + hv \rightarrow O^{\bullet} + O_2 \tag{6}$$

Oxygen radicals readily bond to the diamond film surface, forming an oxygenated layer. As this process is not carried out under vacuum and other unknown samples are placed in the chamber by other personnel, this method of oxygenation can incorporate contaminants into the surface of the sample. Depending on the temperature at which these contaminating species out-gas, they may still be present during the lithium deposition process after a cleaning anneal treatment ($300^{\circ}C$ for $1hour$). Alternative methods of oxygenation include UV-activated ozone in a vacuum chamber. This is the process that was used for $0.5sccm$ NDD samples as was all that was available at the time, samples were able to be kept in an argon chamber for transfer to the lithium deposition chamber and were only exposed to air in the sample mounting process. So contamination should have been minimised compared to samples prepared bu UVO-cleaning.

2.2.iv Ultra-High Vacuum Deposition

Lithium depositions were carried out in the ultra-high vacuum (UHV) platform, NanoESCA. This instrument is also where all anneals, XPS and UPS measurements took place. Within this system, samples are loaded into a chamber used entirely for lithium and tin depositions, cross-contamination from these species is kept minimum due to their separate valve systems and the constantly maintained vacuum of the chamber.
For $30 minutes$ before deposition takes place, the lithium source is degassed to reach the temperature for deposition and maintained at this temperature for $15 minutes$.

Parameter	Value
Temperature	$440°C$
Filament Current	$2.7A$
External Voltage	$2.6V$
Background Pressure	$1 - 2 \times 10^{-9} mBar$
Deposition Pressure	$3 \times 10^{8} mBar$

Table 6: Deposition parameters for lithium deposition using thermal evaporation. The crucible in which lithium sits is subject to filament heating described by the external voltage and filament current. The background pressure is the pressure in the deposition chamber before the lithium source is prepared by out-gassing.

Deposition amounts of lithium were calibrated by depositing an unknown amount on an oxygenated NDD sample with a nitrogen concentration of $0.3 sccm$. XPS measurements were taken before and after deposition so background removal could take place of the spectra focused at the lithium peak. The area underneath the peak was calculated and the electron-cross section was accounted for. Using an attenuation length of $3.8nm$, these values were substituted into the Thickogram equation and graph[86] to obtain the thickness of the deposited film. For a deposition time of $260s$ a thickness of 3.0Å assuming the number density of lithium and carbon is the same on the surface, or 1.0Å assuming lithium adopts it's bulk density where there is roughly one lithium atom for every three carbon atoms at the interface. For this work, as lithium layers a thickness of one monolayer (ML) or less, it is assumed the atoms are not as dense as would be the case for their atoms in a bulk material. Taking a monolayer to equal the length of the lithium unit cell, $0.35nm$ and the deposited amount to correspond to the surface density of lithium, 3.0Å = $0.86ML$, the deposited amount was found to be $1.17ML$. As this was for a $260s$ deposition, the deposition time for $1ML$ of lithium was calculated to be $305s$.

2.3 Absorber Surface

Absorber surface functionalisation is just as important as that of the emission surface for thermionic emission in a simulated solar radiation system.

2.3.i Diamond-Like Carbon

DLC is grown using CVD on the underside of the molybdenum substrate to act as a black-body radiation absorber. This DLC layer is produced in the same way as the diamond films in this study but with a different set of growth conditions.

Parameter	Value
Methane Concentration	$25 sccm$
Hydrogen Concentration	$300 sccm$
Nitrogen Concentration	$1.5 sccm$
Pressure	$140 Torr$
Power	$1.5 kW$
Temperature	$1200°C$
Time	$3 hours$

Table 7: Growth conditions and parameters of the DLC layer grown using the method of CVD as with the diamond films grown and described in this work. Such conditions demonstrate how small changes in the growth parameters can lead to surfaces very different to pure synthetic diamond and how crucial they are in achieving high-quality samples.

2.3.ii Alternative Methods

Higher-performing absorber surfaces can be produced by laser-etched gratings of regular patterns on the underside of the sample. Such patterns improve thermal absorbance up to 90% in the visible range.[87] Laser-etched absorber surfaces would be more desirable for the emission surfaces developed in this work but were beyond the scope of this project in terms of both time scale and availability of such lasers capable of producing the cut pattern.

2.4 Nomenclature

For simplicity in this work, each functionalisation has been reduced to a few letters to ease the labelling process throughout. Described in the table below are the aforementioned abbreviations and their meanings.

Abbreviation	Meaning
NDD	**N**itrogen-**D**oped **D**iamond
DLC	**D**iamond-**L**ike **C**arbon
H	**H**ydrogen termination
OLi	**O**xygen-**Li**thium termination

Table 8: This table describes the abbreviations used in this work to annotate the various sample components used throughout this work in the interest of simplicity.

Abbreviation	Resulting sample
NDD	**N**itrogen-**d**oped **d**iamond on molybdenum substrate
NDD+DLC	**NDD** sample with **DLC** absorber surface
NDD+DLC+H	**NDD** sample with **DLC** absorber surface, terminated with **h**ydrogen
NDD+DLC+OLi	**NDD** sample with **DLC** absorber surface, terminated with **o**xygen and **li**thium

Table 9: This table shows the sample labels used throughout this work as a result of the individual component abbreviations, and their descriptions.

3 Analytical Methods and Results

3.1 Surface Quality and Morphology

3.1.i X-Ray Photo-emission Spectroscopy

In photoemission spectroscopy, photons from the source of a chosen wavelength, are absorbed by electrons within the material, if the energy of the incident photon is sufficient to remove the electron then the electron is emitted from the surface with kinetic energy described by the photoelectric effect as described in Equation 1. The emitted electron and its remaining kinetic energy are analysed by the detector. Hence, the wavelength and energy of the light source determines what can be analysed within the sample, whether that be surface composition in the case of XPS or electronic structure in UPS. The binding energy can be deduced from the kinetic energy of the photoelectrons and the energy of the light source.

$$E_{bin} = E_{photons} - E_K \tag{7}$$

In the case of XPS, the X-ray light source excites electrons from the core energy levels, giving the bonding energies of surface atoms to indicate the chemical composition of the sample.[28] Spectroscopy techniques like the XPS and UPS methods described in this work are carried out under UHV to ensure unimpeded travel of emitted photoelectrons to the detector, this ensures accurate analysis of the electron energies.
XPS spectra were obtained for NDD samples with a nitrogen concentration of $0.3 sccm$. One of these samples was used to calibrate the lithium deposition system to calculate the thickness of the terminated layer, the other sample was terminated with half ML (HML) coverage of lithium.

Spectra were obtained for both pre- and post-deposition of lithium to identify any contaminants at both stages as well as to obtain an indication of inter-layer bonding from the attenuation of characteristic peaks of the species involved.
Parameters for XPS measurements are as follows: $-0.5eV$ $0.25s$ step energy and time with a sweeping energy of $100eV$ for surveys, and $-0.05eV$ $0.5s$ step energy and time with a sweeping energy of $50eV$ for energy-focused spectra. Following are the spectra obtained for the calibration sample, prepared in the standard method of this work as described in 2.2 as are all samples under XPS testing, the only difference being their resulting lithium terminations.

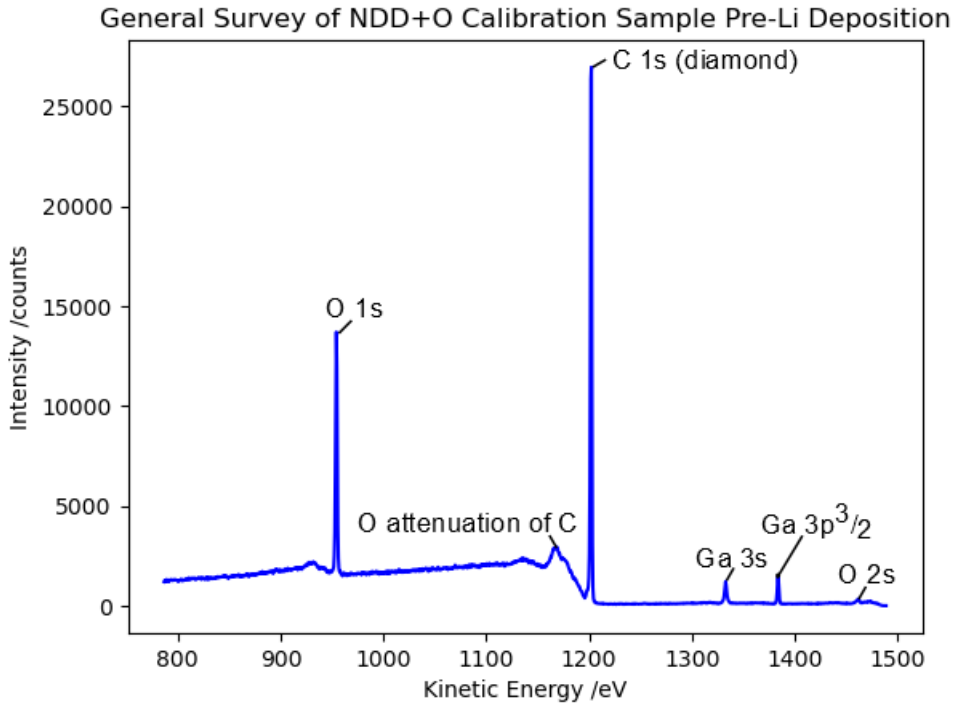

Figure 18: General survey of an electrostaticaly nucleated 0.3sccm NDD sample terminated with ML coverage of oxygen via UV-ozone exposure. This spectrum was obtained after a pre-cleaning anneal treatment at a temperature of 300°C for 1 hour.

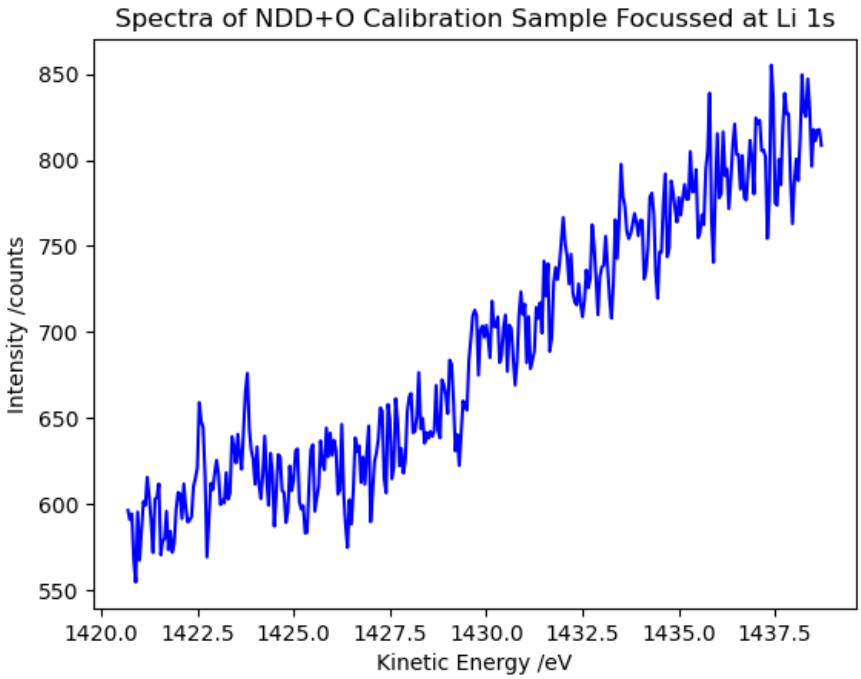

Figure 19: Spectra obtained for an electrostaticaly nucleated 0.3sccm NDD sample terminated with ML coverage of oxygen via UV-ozone exposure. This spectrum was obtained after a pre-cleaning anneal treatment at a temperature of 300°C for 1 hour.

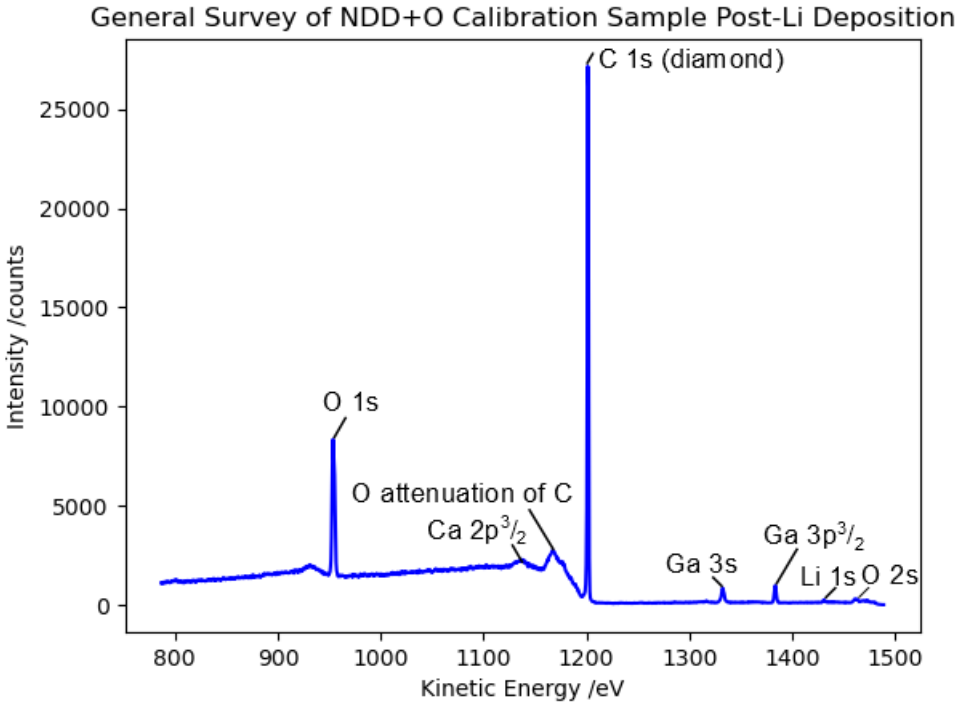

Figure 20: General survey of an electrostaticaly nucleated 0.3sccm NDD sample terminated with ML coverage of oxygen via UV-ozone exposure, terminated with lithium at 440°C and annealed at a temperature of 500°C for 1 hour.

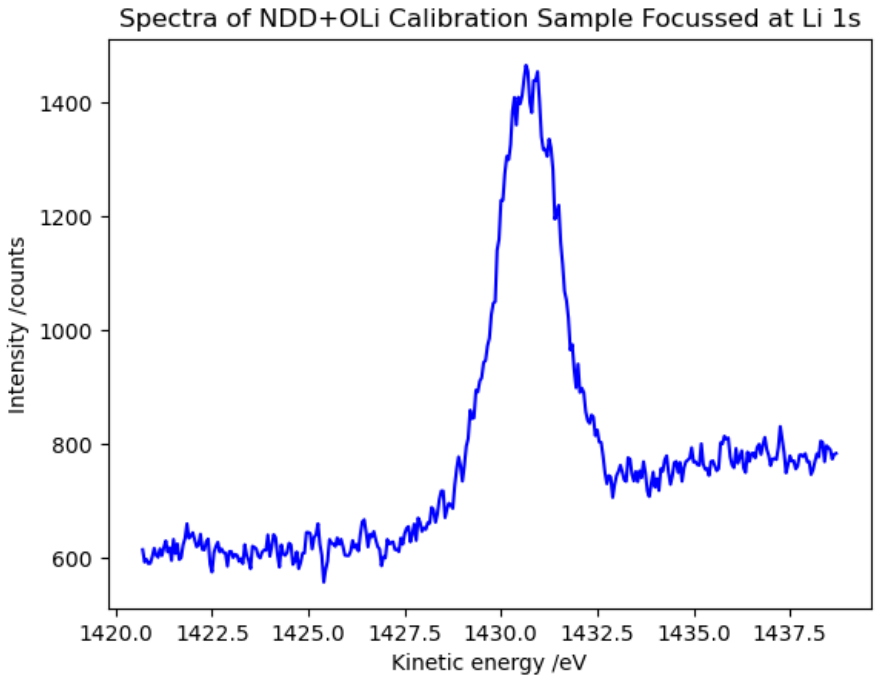

Figure 21: Spectra obtained for an electrostaticaly nucleated 0.3sccm NDD sample terminated with ML coverage of oxygen via UV-ozone exposure, terminated with lithium at 440°C.

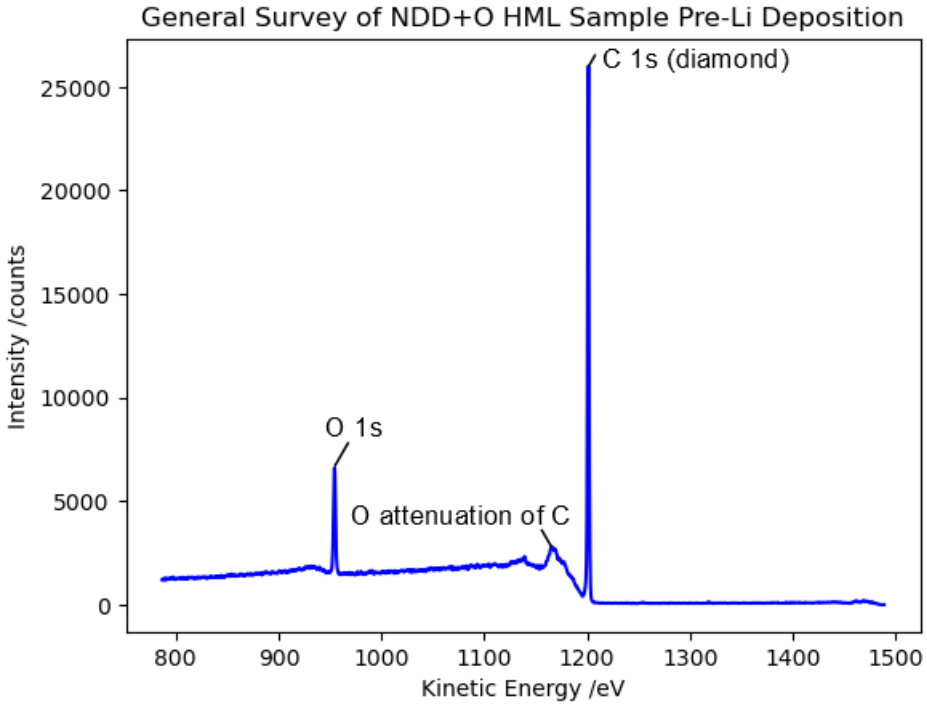

Figure 22: General survey of an electrostaticaly nucleated 0.3sccm NDD sample terminated with ML coverage of oxygen via UV-ozone exposure. This spectrum was obtained after a pre-cleaning anneal treatment at a temperature of 300°C for 1 hour.

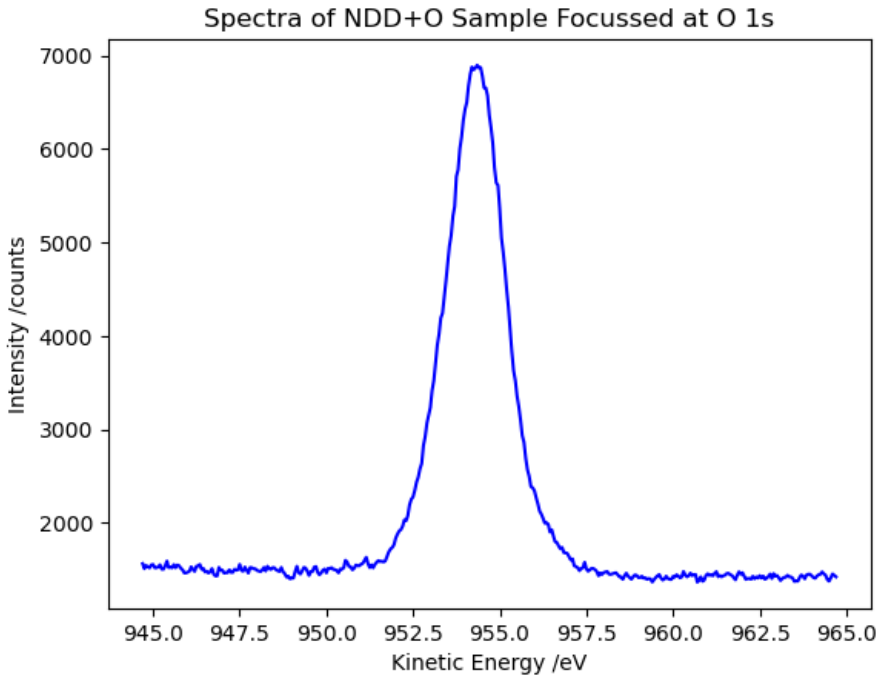

Figure 23: Spectra obtained for an electrostaticaly nucleated 0.3sccm NDD sample terminated with ML coverage of oxygen via UV-ozone exposure.

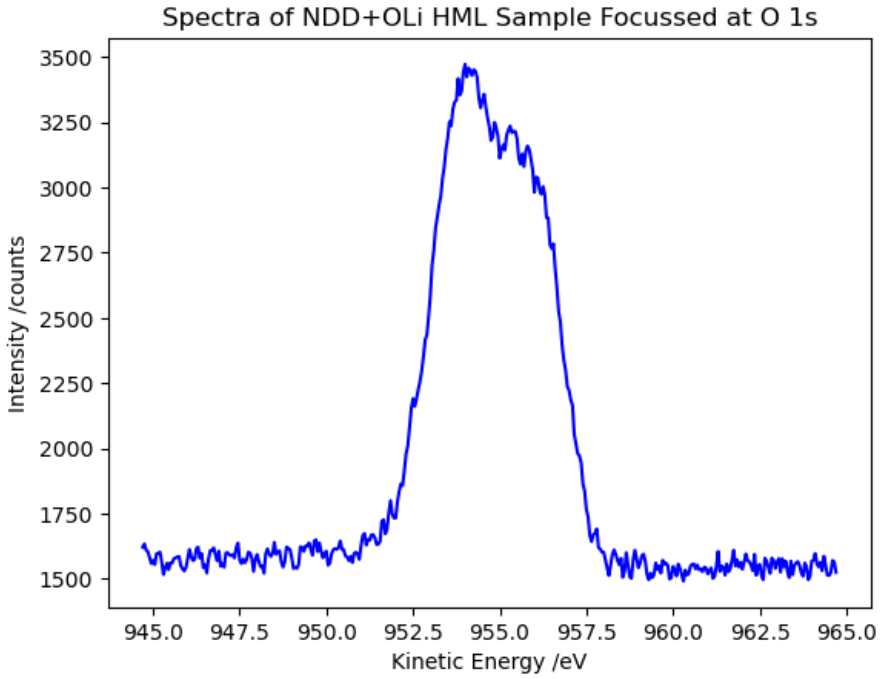

Figure 24: Spectra obtained for an electrostaticaly nucleated 0.3sccm NDD sample terminated with ML coverage of oxygen via UV-ozone exposure, terminated with HML coverage of lithium at 440°C.

3.1.ii Discussion

Visual analysis of the spectra suggests that the carbon peak is not being attenuated by the lithium peak, suggesting little-to-no bonding occurs between these two species.
The oxygen peak, as seen in 23 and 24, exhibits attenuation after lithium deposition but not before, confirming that the two surface layers have bonded with some degree of strength.
Attenuation of the carbon peak towards the energy of the oxygen peak suggests carbon-oxygen bonding at the surface of the diamond. This is concurrent with conclusions made by Martin (2011)[28] where it was also concluded that lithium mainly bonds to surface oxygen atoms and not to bulk diamond.
Suspected gallium peaks have been observed in the spectra of the calibration sample, most likely from the UV-ozone chamber from the use of other personnel with such a contaminated sample. Gallium can be highly reactive and react with alkali metals, this could affect the strength of bonding between lithium and oxygen, thus affecting both the physical and electronic structure of the terminated layer, both of which characteristics are crucial for thermionic emission.

3.2 Electron Energy Distribution

Electron energy distributions of four samples were obtained using UPS in the UHV instrument, NanoESCA.

3.2.i UV Photoemission Spectroscopy

The process behind UPS follows the same mechanism as that for XPS, however, due to the different energies of the light sources it gives different information about the material. As ultraviolet (UV) photons have higher energies than x-ray photons, they are capable of probing valence band electrons giving the electron energy distribution of the sample under study.[28]

Four samples were investigated with UPS; $0.3sccm$ and $0.5sccm$ NDD samples, each with both HML and FML Li terminations. Due to time constraints and maintenance of preferred equipment, the two sets of samples were prepared slightly differently: $0.3sccm$ NDD samples were seeded by electrostatic nucleation and oxygen terminated in the UVO-cleaner, $0.5sccm$ NDD samples were seeded by manual abrasion and oxygen terminated in a UV-activated vacuum chamber. Nucleation differences in the two sets of samples should have little effect on diamond growth, but as the concentrations differ it is difficult to say with certainty whether the differences arise from the seeding method or the changes in nitrogen content. Theoretically, the seeding method should only affect the quality of the diamond film in terms of its adhesion to the substrate, which was uniform for all samples, no delam-

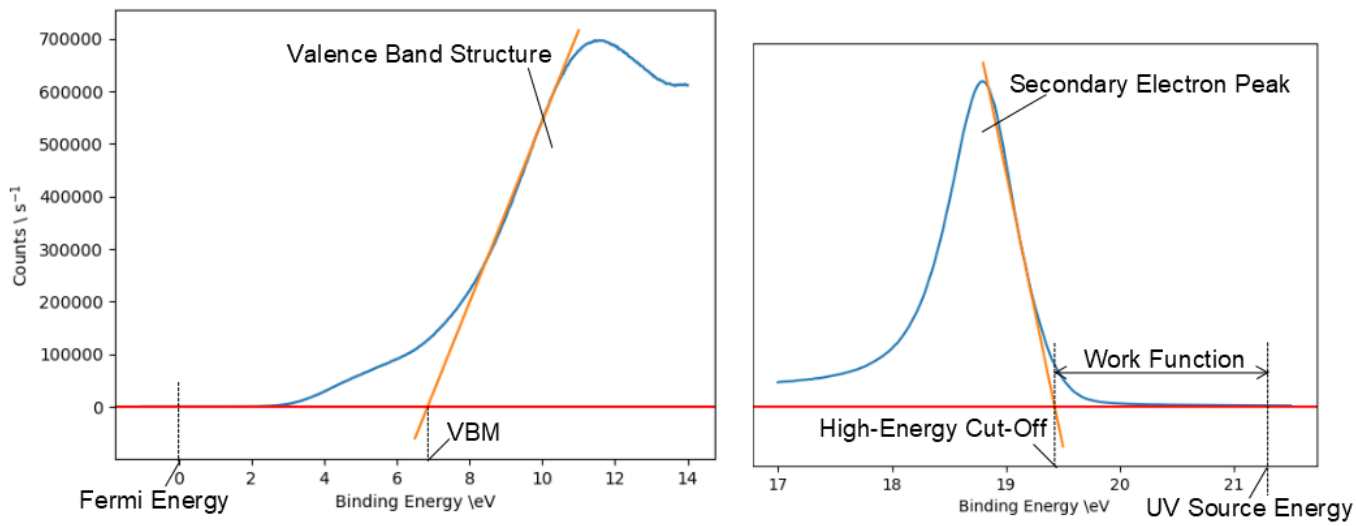

Figure 25: Shown here is an annotated example of a spectrum obtained from a UPS measurement. This visually explains the features which will be discussed in this section.

ination occurred. However, the $0.5sccm$ samples were visually different compared to the $0.3sccm$ samples, the surface had a rougher morphology almost giving the sample a banded pattern. This pattern could be a result of the underlying manual abrasion or could be considered a result of the increased nitrogen content. Increasing nitrogen concentration in a diamond film adversely affects the diamond structure and so increases graphitic content in the film, hence the appearance of darker regions giving the 'banded' appearance. Thus, the formation of these 'bands' is most likely a result of graphite formation within the film, the location of which would presumably be at the sites of concentrated nucleated diamond caused by the non-uniform nature of manual abrasion, that would otherwise (in the case of lower nitrogen concentrations) cause no issue in the resulting surface morphology.

It is important to note that the following samples were removed from the vacuum after lithium depositions for $1week$ before UPS measurements were taken. So, samples have been exposed to air and will have some level of contamination, although the presence of the terminated oxygen layer theoretically should increase the strength of bonding of lithium to the surface, the actual effects of this have not been studied in this work, so how readily the surface lithium reacts with the environment is not known for certain. XPS measurements before those taken for UPS would give the binding energies of the specific contaminants as well as the thickness of the lithium layer to determine the level of desorption due to its reaction with air. Contamination of the following samples will present itself in deviations from the expected shapes of the UPS spectra, especially at the VBM and high-energy cut-off.

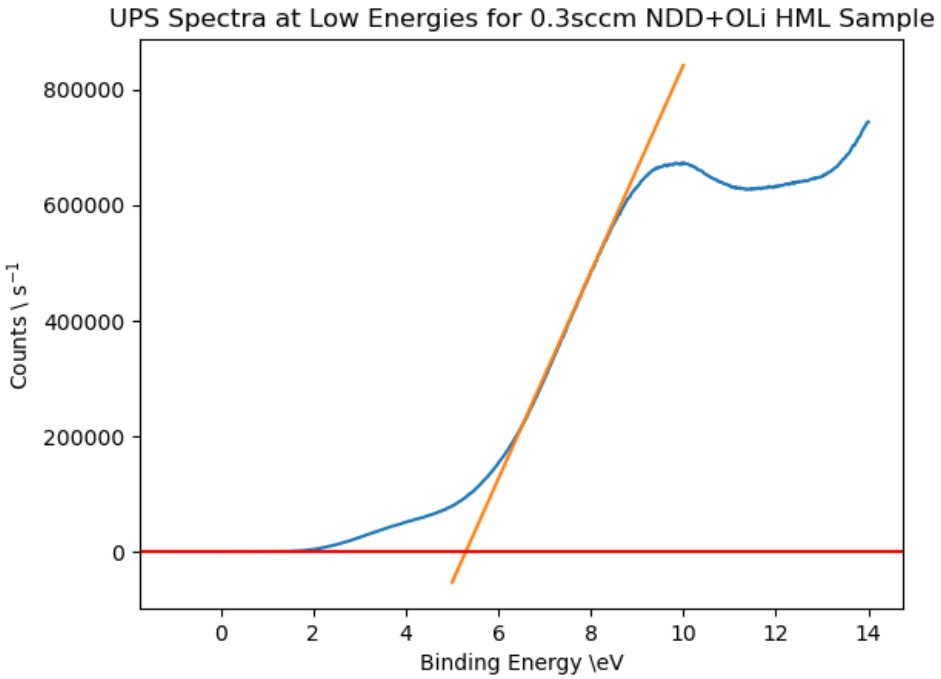

Figure 26: UPS spectra of an NDD sample (N concentration: 0.3sccm) terminated with HML coverage of Li on an oxygenated surface at low binding energies. The VBM was estimated to be 5.29eV.

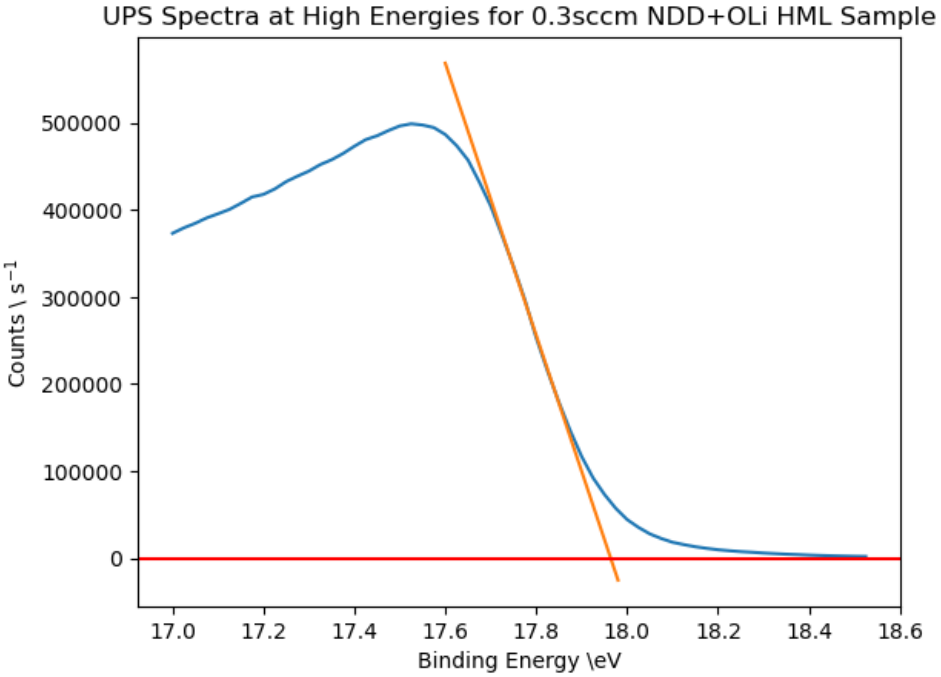

Figure 27: UPS spectra of an NDD sample (N concentration: 0.3sccm) terminated with HML coverage of Li on an oxygenated surface at the secondary electron peak. The high-energy cut-off was estimated to be 17.96eV.

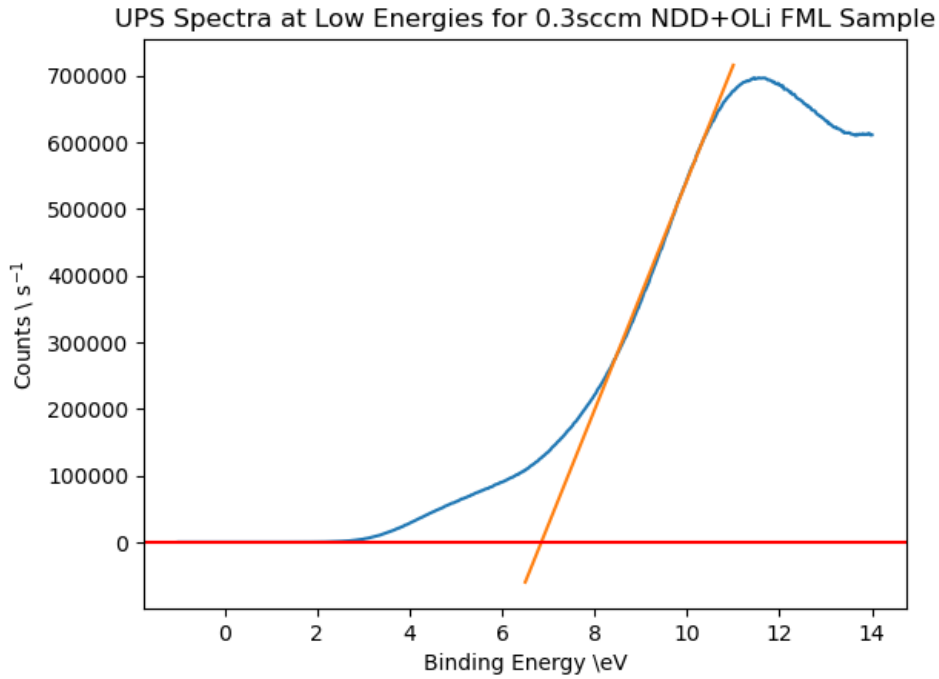

Figure 28: UPS spectra of an NDD sample (N concentration: 0.3sccm) terminated with FML coverage of Li on an oxygenated surface at low binding energies. The VBM was estimated to be 6.85eV.

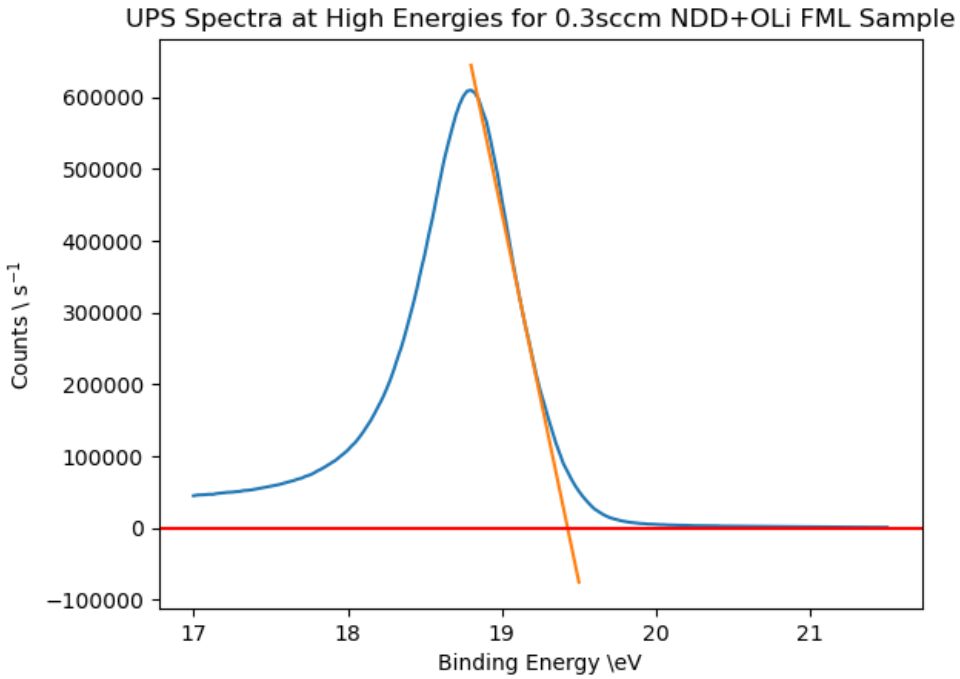

Figure 29: UPS spectra of an NDD sample (N concentration: 0.3sccm) terminated with FML coverage of Li on an oxygenated surface at the secondary electron peak. The high-energy cut-off was estimated to be 19.43eV.

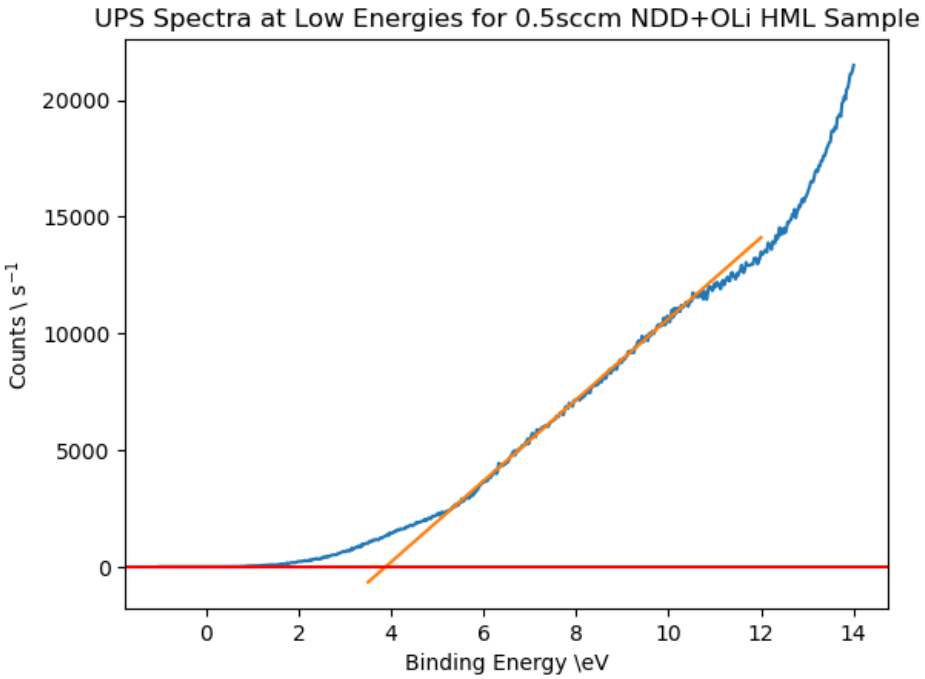

Figure 30: UPS spectra of an NDD sample (N concentration: 0.5sccm) terminated with HML coverage of Li on an oxygenated surface at low binding energies. The VBM was estimated to be 3.88 eV.

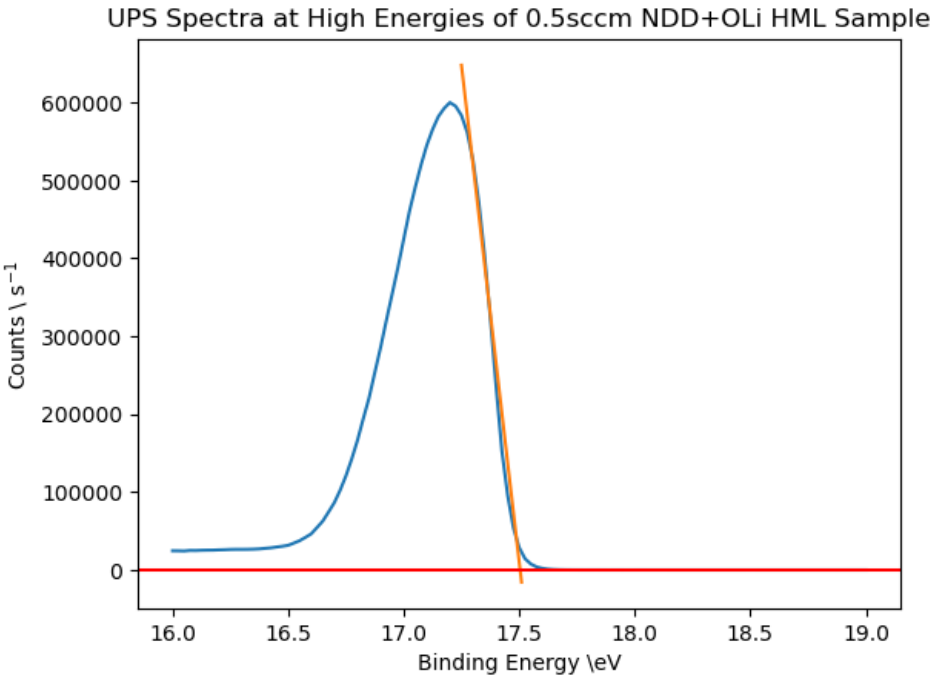

Figure 31: UPS spectra of an NDD sample (N concentration: 0.5sccm) terminated with HML coverage of Li on an oxygenated surface at the secondary electron peak. The high-energy cut-off was estimated to be 17.50eV.

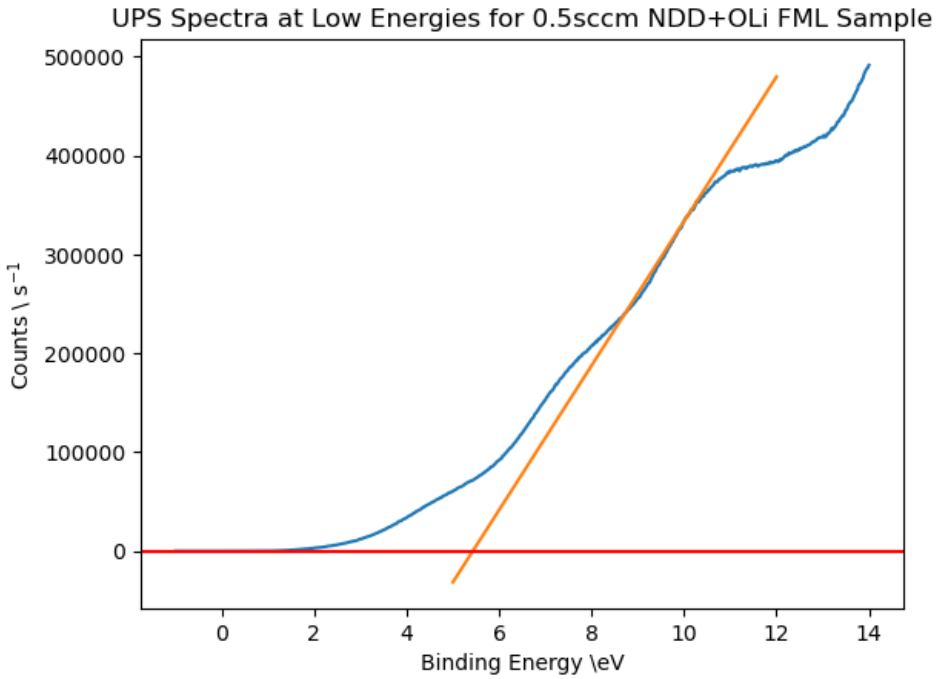

Figure 32: UPS spectra of an NDD sample (N concentration: 0.5sccm) terminated with FML coverage of Li on an oxygenated surface at low binding energies. The VBM was estimated to be 5.43 eV.

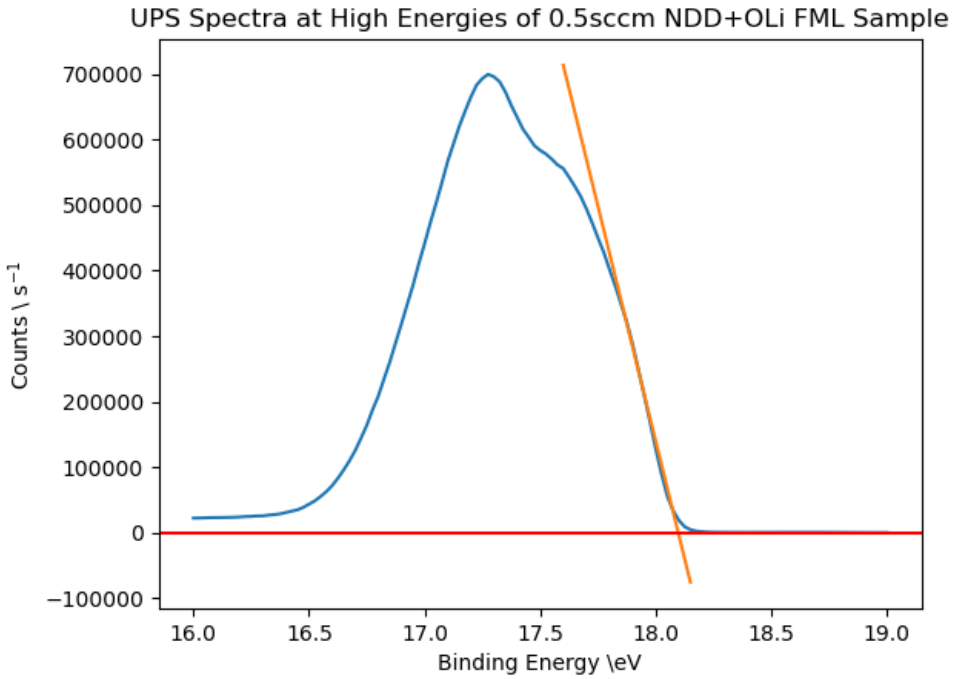

Figure 33: UPS spectra of an NDD sample (N concentration: 0.5sccm) terminated with FML coverage of Li on an oxygenated surface at the secondary electron peak. The high-energy cut-off was estimated to be 18.01eV.

Sample	VBM $/eV$	High-Energy Cut-Off $/eV$	Work Function $/eV$
0.3$sccm$ NDD+OLi (HML)	5.29	17.96	-3.26
0.3$sccm$ NDD+OLi (FML)	6.85	19.43	-1.79
0.5$sccm$ NDD+OLi (HML)	3.88	17.50	-2.72
0.5$sccm$ NDD+OLi (FML)	5.43	18.10	-3.12

Table 10: Tabled values of the measured VBM and high-energy cut-off for the samples from UPS spectra obtained under vacuum once the samples had been exposed to air for 1 week. The work function was calculated using the high-energy cut-off and the energy of the UV light source (He lamp).

Work function estimations were calculated by first calculating the high-energy cut-off, the point of intersection between the x-axis (shown in red on the graphs) and the tangential line (shown on the graphs in orange) to the secondary electron peak. This point of intersection gives the high-energy cut-off, the maximum energy of electrons in the sample. To find the work function, the photon energy is subtracted from this value.[28,88]

$$\phi = E_{cut-off} - E_{photon} = E_{cut-off} - 21.22eV \tag{8}$$

As can be seen by the varying degrees of gradient reduction, this high-energy cut-off point could vary in value depending on the position at which the tangent is calculated, this does introduce an error in the exact value of the work function. For this reason, all tangents have been calculated for the gradient of the peaks in the centre of the slopes, ensuring maximum contact of the tangent with the curve. This consistency should help improve the precision and comparability of obtained values for all samples. The position of the VBM was calculated in a similar way, the point of intersection between the x-axis (red) and the tangential line (orange) at low energies of the UPS spectrum, gives the energy of the VBM.

3.2.ii Discussion

Apart from the spectrum obtained for the 0.5$sccm$ NDD sample with FML Li coverage, the high energy spectra of the samples under test had uniform shapes and exhibited only one peak maxima. The aforementioned sample had a non-symmetric secondary electron peak, this could be due to a few causes for distortion of the shape of the peak; the sample contains contaminants at higher energies compared to the other samples although it's contaminants should be comparable with the other 0.5$sccm$ NDD sample, another possible reason is charging of the sample during the measurement process. A secondary light source of mercury was needed to counteract the charging effects of the sample during the UPS process, this could have been due to a faulty sample holder causing a poor electrical connection or due to a lack of complete conductivity of the sample due to the increased nitrogen con-

centration as well as, or due to increased topography. The mercury lamp was used for all samples but that does not ensure the occurrence of uniform charging for all measurements.

UPS measurements usually take place at an extraction voltage of $12V$, however, for these samples the resulting electron emission was too 'bright' for the detectors and would have caused both damage to the detector and non-physical broadening of the electron energy distributions. For the $0.3sccm$ and $0.5sccm$ NDD samples, an extraction voltage of $6V$ and $4V$ respectively.

These were the largest extraction voltages possible to use for these samples, however, if the extraction voltage is too low, the electron distribution will be narrower as a result of an incomplete collection of emitted electrons. All but one ($0.3sccm\ FML$) sample had a maximum binding energy of $18eV$ and all samples had a similar minimum binding energy of $4eV$. There are two possible reasons for these similar energy ranges: this narrowing effect as a result of reduced extraction voltages played a minimal or negligible role in the energy distribution of emitted electrons, as each set of samples had a different extraction voltage but their range was unchanged however this suggests all samples have a similar high-energy cut-off so all have a similar work function despite their differences which seems unlikely; the other explanation is that the spectra for $0.5sccm$ NDD samples have been energetically narrowed and so their high-energy cut-offs and resulting work functions are greater than calculated from their respective graphical data which is to be expected from poorer quality diamond as a result of increased nitrogen concentration increasing the graphite content of the sample.[6]

It is difficult to tell which of these explanations represents the physical reality of these samples, thermionic emission testing, by comparing the resulting emission currents, of each sample would indicate whether the work functions are indeed similar or whether the energy scales have been skewed. It remains that values extracted from the graphical data are subject to error as a result of contaminants altering the shape of the profiles, as well as the position of the tangential line. However, the calculated values of the work function can give an estimation of the realistic values.

Repeating these measurements before and after OLi termination at the same extraction voltages would aid in the investigation of the physicality of the energy scales as that of the bare diamond could be used to extract the work function of the surface to be compared with values in literature (WF: $6.1eV$ of bare diamond)[28]

[28] Ullah (2023)[27] found work functions of $3.93eV$ for oxygenated, lithiated single crystal diamond doped with boron, the thickness of this lithium layer is assumed to be sub-ML. This value is slightly higher than was calculated from UPS spectra obtained in this work. Boron is a p-type promoting species so acts as an electron acceptor within the material, which as a result leads to better conduction due to the increased hole population within the crystal

lattice. Although this increased conduction would improve thermionic emission pathways, the boron would not provide an electron population to the surface as nitrogen would, so the VBM for the NDD sample should be greater than that of the boron-doped diamond (BDD). The level of band bending is determined by the strength of the oxygen-lithium dipoles on the sample surfaces and results in the new WF. For the NDD and BDD samples, the WF should be similar if the thickness of the deposited lithium layer is the same. As the two samples were prepared and processed in different ways (BDD samples were purchased, the oxygenation method is unknown and all UPS measurements were taken under vacuum), different levels of contamination for the two samples may lead to varying levels of strength for the oxygen-lithium surface dipoles, however, it seems that the NDD samples would be subject to more contaminants due to their exposure to air before UPS measurements were taken, but the lack of XPS spectra for these samples leaves these theorised contaminants and their quantities unknown. Thus, as the NDD sample surfaces have theoretically been compromised it is their WFs that should be higher than that of the BDD sample but this is not the case.

The WF value found by Ullah (2023)[27] is greater than that found in this work for either tested nitrogen concentration or lithium thickness. Sample contaminants should increase the WF instead of reducing it, suggesting the NDD samples may not be as contaminated as suspected. Due to the discussed similarities and differences of these samples, it could be concluded that the nitrogen incorporation into the diamond lattice is what has led to the increased reduction in WF compared to a BDD sample also terminated with oxygen and lithium. This may be due to the increased Fermi level within the NDD material as a result of the increased electron population that contributes to the reduction of the WF. Martin (2011)[28] studied lithium and oxygen terminations on diamond samples both theoretically and experimentally. They used UPS measurements to calculate the work functions of boron-doped single-crystal diamond substrates terminated with either hydrogen, oxygen or both oxygen and lithium, resulting WFs for these samples were $3.62eV$, $5.3eV$ and $2.8eV$ respectively. Lithium coverage in this case was a full ML. In their theoretical studies carried out by density functional theory (DFT), both the (111) and (100) diamond orientations were studied with oxygen-lithium terminations for both ether and carbonyl oxygen bonding configurations. For (111) diamond orientations and with the carbonyl and ether oxygen configurations respectively, HML Li coverage yielded WFs of $-2.84eV/-4.23eV$ and $-3.17eV/-1.87eV$, FML lithium coverage yielded WFs of $-1.39eV$ and -3.36. For (100) diamond orientations, HML and FML lithium coverages respectively yielded WFs of $-2.7eV/-1.87eV$ and $-4.52eV/-3eV/-2.3eV$. Where two values are available for the WF, there are two possible bonding configurations of the lithium to the oxygen layer.

Experimental values for the WF found in the above study for a BDD+OLi (FML) sample were greater than that found for NDD+OLi ($0.3sccm$, FML) samples in this study ($+1.01eV$)

and less than that found for NDD+OLi($0.5sccm$, FML) samples ($-0.32eV$).This suggests the presence of nitrogen contributes to the electronic structure of the diamond material in such a way as to reduce the work function. This also adds to the speculation within this work that $0.5sccm$ nitrogen concentrations produce poor-quality diamond material and, in doing so effects both the physical and electronic pathways for the emission of electrons. In terms of the theoretical study described above, there is a general trend where for the ether-bonded oxygen, the WF for HML lithium coverage is lower than that of the FML lithium coverage. Conversely, the WF found for the carbonyl-bonded oxygen was greater in the HML lithium coverage than that of the FML lithium coverage. Comparing this trend with experimental data collected in this work, it could be suggested that for the lower concentrations of nitrogen in the diamond film ($0.3sccm$), oxygen on the surface is in the carbonyl configuration, and for higher concentrations of nitrogen ($0.5sccm$) where the diamond is of poorer quality, surface oxygen is in the ether configuration. As the NDD samples are polycrystalline, it is difficult to identify the singular effect of the diamond orientation.

From the comparisons of work function estimations made in this work and those found both experimentally and theoretically by others in the field, it seems as though NDD has been successful in reducing the WF of oxygen-lithium terminated diamond, with respect to BDD samples and bare diamond surfaces.
Further investigation into the resulting emission currents would be an interesting progression as currents as high as $2mA$ were found by Ullah (2023)[27] for the BDD+OLi samples.

3.3 Thermionic Emission Current

3.3.i Thermionic Emission Kit (TEK)

Emission currents of a $0.3sccm$ NDD sample with two types of surface termination, hydrogen and oxygenated lithium (HML lithium coverage) have been investigated, these parameters for nitrogen and lithium content have been chosen as the former yields higher quality diamond and the latter is theorised to produce the lowest WF. The thermionic emission kit (TEK) is comprised of an IR ($150W$ $1500nm$) laser incident to a sample stage within a vacuum chamber, where the sample stage is connected to an external voltage.

Samples are placed onto a sample mounting and held in place with molybdenum contacts. These contacts are connected to the electrical contacts of the sample stage using molybdenum wire. Ensuring the positive and negative terminals remain unconnected, the sample mounting is moved closer to the collector attached to the sample stage. The sample stage is placed within the emission detection chamber and the system is brought to vacuum pressures (10^{-8}). The sample is heated using an IR ($15000nm$) laser, this heats the underside of

the sample (the absorber surface) and induces electron emission from the sample, collected by the collector. The temperature of the sample is measured using a two-colour pyrometer. An external bias is applied across the system to ensure a continual flow of electrons. Keeping the chamber under vacuum is not only important to both reduce thermal losses and try to keep the two electrodes thermally insulated from one another, but also to allow for easy electron flow between the two plates.
A DLC layer was grown underneath an NDD sample ($0.3 sccm$) and subjected to a hydrogen plasma to terminate the surface. Hydrogen is a common and fairly effective NEA-imparting terminant[89,4,2] so the resulting emission current of this sample configuration was first tested to compare with values found in the literature to assess the quality of the surface.
It is important to note that the sample under investigation in this section did not undergo XPS testing, but was prepared in the same way as those that did. Therefore, it is not unreasonable to suggest that the carbon-oxygen-lithium bonding described by the XPS spectra is representative of this sample, however, it cannot be stated with absolute certainty. Any anomalous contaminants not found in other samples can also not be identified as with their potential effects on the WF and NEA of the sample. Such contaminants may have arisen from highly contaminating species in the UVO-cleaner or from the sample holders used in NanoESCA.

3.3.ii Nitrogen-Doped Diamond with Hydrogen Termination

Hydrogen on diamond surfaces desorbs at temperatures around $700°C$[90] so a maximum temperature of $725°C$ was first tested. Prior to the two tests carried out on the hydrogen-terminated NDD sample, the sample must be thermally activated. This involves slowly heating the sample to a safe (non-desorbing) temperature to initiate the conductivity of nitrogen within the sample. Slow initial heating also reduces damage to the sample, especially to the DLC absorber surface that has the potential to delaminate. Configuring the position of the two-colour pyrometer can also happen at this activation stage.
For the profile below (Figure 34), the sharp spikes in temperature (red line and axis) result from the change in position of the pyrometer. 'Steps' in the temperature profile are from manual increases in the set temperature of the laser. The emission current (blue line and axis) shows a relatively large amount of noise around $300°C$, these values fluctuate from positive to negative around zero so are not representative of physical electron emission. It can be seen that electron emission begins around $600°C$, at this stage the whole sample has been fully heated and has activated the n-type conductivity of the embedded N atoms once the threshold temperature has been met and maintained for some time ($40 minutes$).

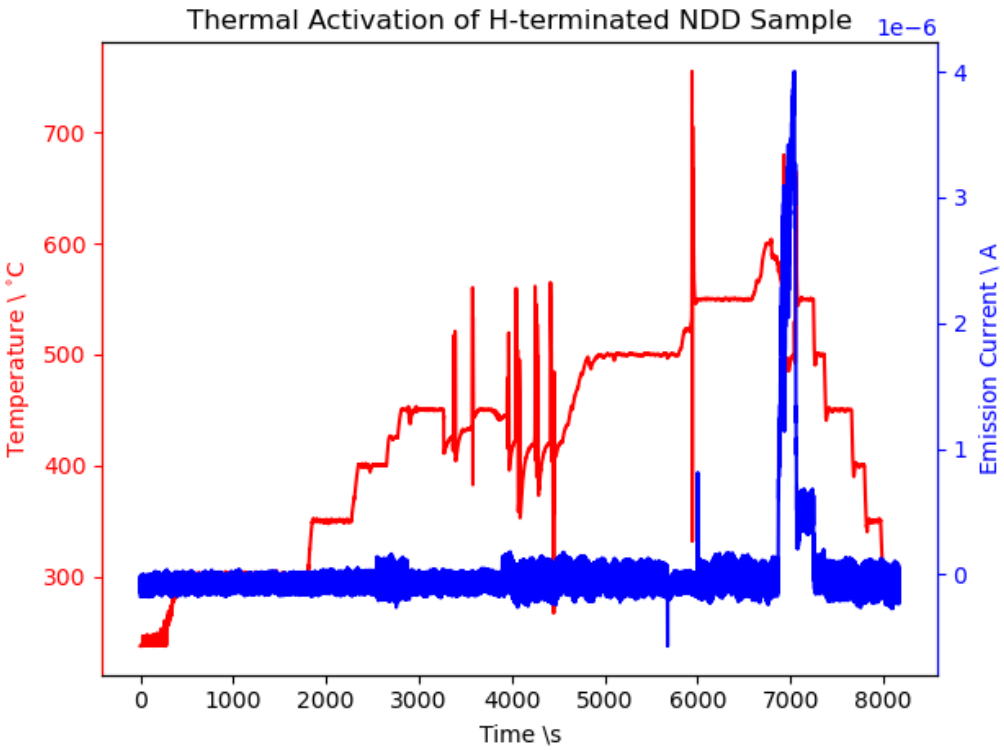

Figure 34: Shown here is the thermal activation of the NDD (0.3sccm) sample with a H-termination, using DLC as an absorber surface.

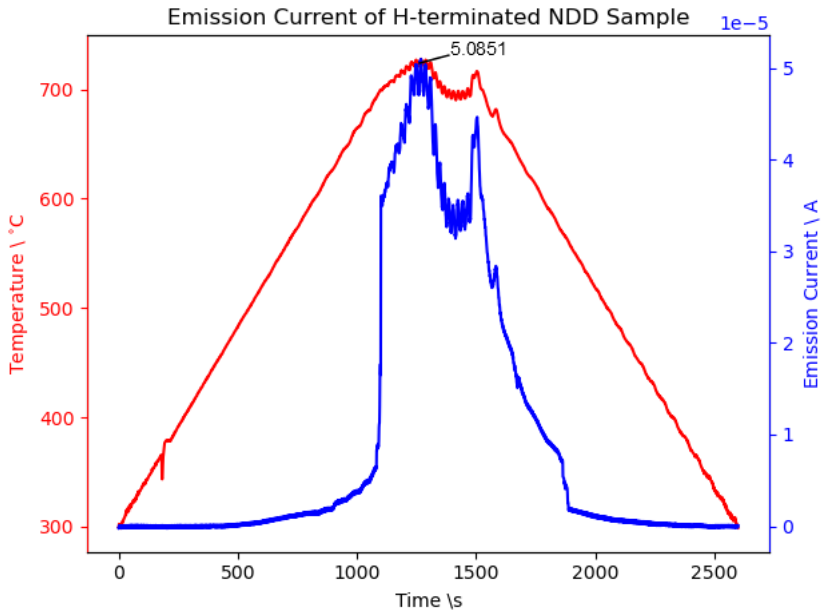

Figure 35: Shown in this graph is the emission current of the same sample (NDD+HT+DLC) once it has been thermally activated.

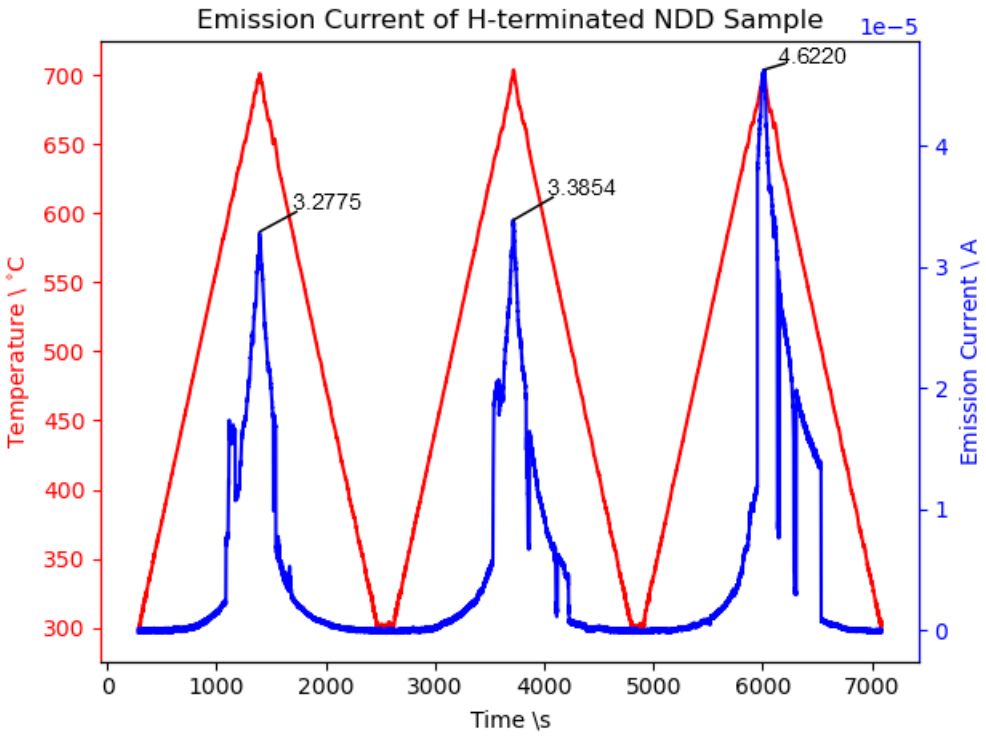

Figure 36: This set of results comprises three temperature cycles reaching a maximum temperature of 700°C. The emission current reaches a new maximum after the third cycle. Irregularities in the emission current profile are most likely due to changes in the surface of the sample hence in the electron structure and transport at the surface.

For Figure 35, a triangular temperature profile has been chosen for this test to investigate the maximum temperature the sample can reach with the DLC absorber. The non-triangular peak of the temperature profile indicates the sample was unable to reach the maximum set temperature of $725°C$, so $700°C$ was chosen for the next test. For this test, as well as the thermal activation of the sample, emission started at around $600°C$. The non-symmetric nature of the peak of the emission current profile reflects the inconsistency of the sample temperature. The maximum emission current for the hydrogen-terminated sample was achieved in the third cycle of testing. This increase is presumably due to either surface reconstruction after sustained heating or the total sample surface had not been fully activated. As emission has been shown to decrease with hydrogen desorption[90] and no hydrogen has been added to the surface, it is reasonable to assume that this increase in emission is not due to surface reconstruction. It is possible that the whole surface had not been completely thermally activated, especially once the shapes of the emission profiles are taken into account, sharp drops in current and non-symmetric profiles suggest a non-uniform surface leading to irregular emission, this would explain the difficulty in successfully heating the whole surface during the activation stage.

3.3.iii Nitrogen-Doped Diamond with Lithium-Oxide Termination (NDD+OLi)

After thermionic testing of the NDD+DLC+H testing, the hydrogen layer was desorbed as a result of high-temperature heating. The sample was kept in a UV-activated ozone chamber to achieve an oxygen termination of the surface ($1ML$) before half a monolayer of lithium was deposited using the NanoESCA UHV platform.

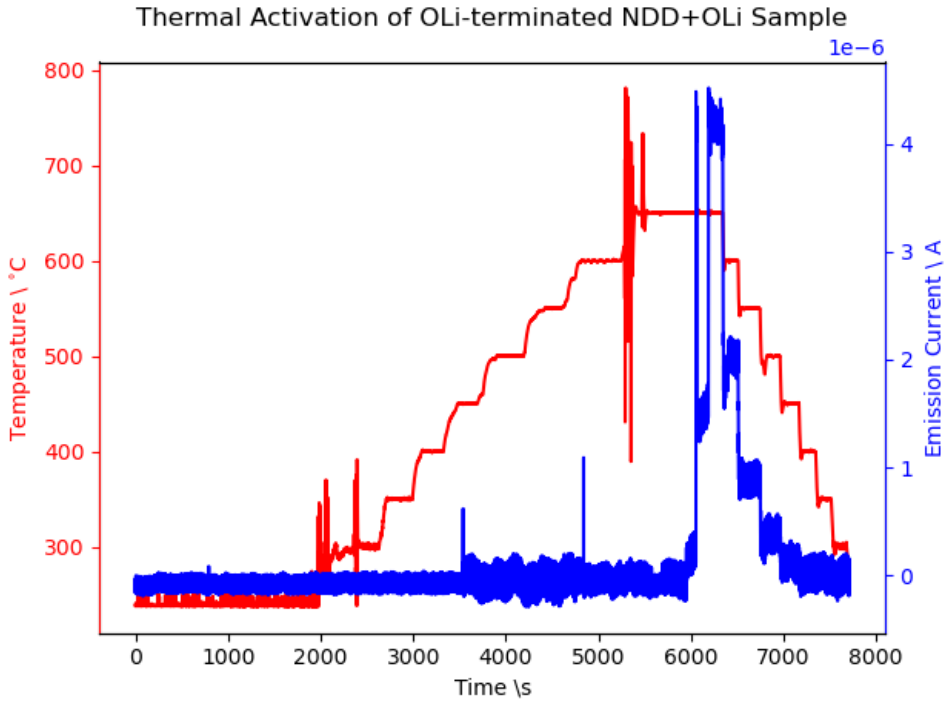

Figure 37: This graph shows the thermal activation of the NDD+DLC+OLi sample.

For the activation cycle in Figure 37, as with the NDD+DLC+H sample, spikes in the profiles show movement of the pyrometer, and the temperature was manually increased in increments as described by the step-like shape of the profile. Emission began at $650°C$. Fluctuations in emission current around zero are as previously described. Temperatures greater than $700°C$ were avoided as it is at this temperature that oxygen-lithium species begin to degas and desorb from the surface. For Figure 38 Emission profiles are generally smooth, suggesting the surface structure is relatively uniform, leading to uniform electron transport. A generally increasing emission current trend can be seen, a deeper discussion of which is to follow.

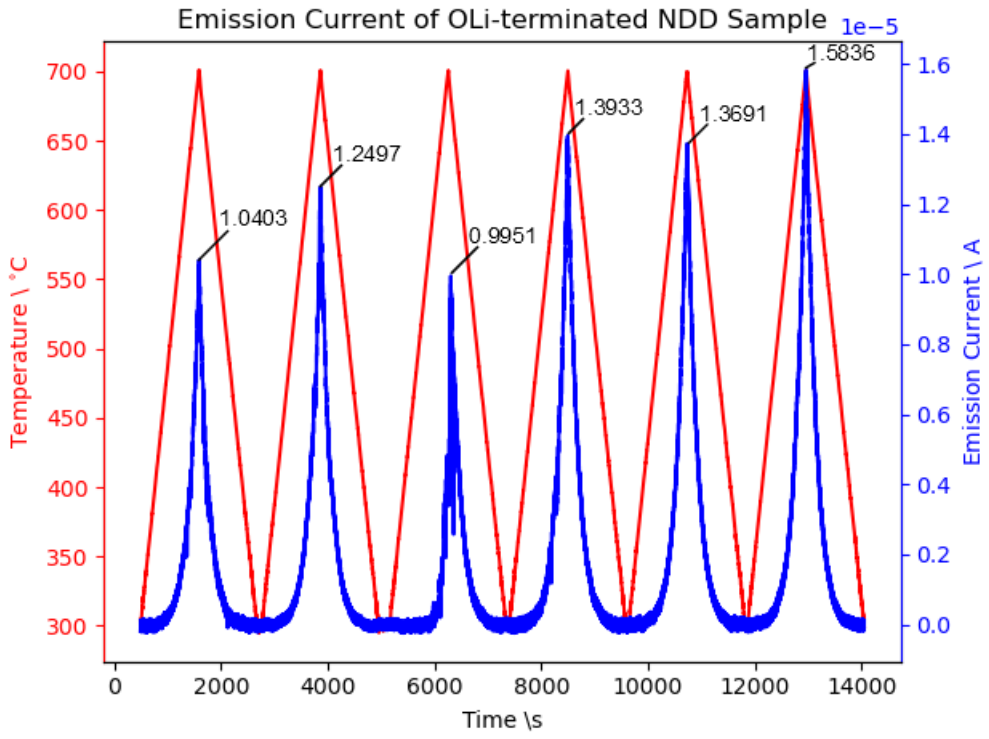

Figure 38: Here shows six cycles of annealing on the NDD+DLC+OLi sample up to 700°C.

3.3.iv Discussion

Termination	T_{max} /°C	I_{max} /mA	x /nm
H	700	0.046220	120
H	725	0.050851	120
OLi	700	0.015836	100

Table 11: Displayed maximum emission currents (I_{max}) yielded from each sample at their given maximum temperatures (T_{max}).

The hydrogenated surface in this work achieved a maximum emission current of $0.051mA$. Zulkharnay (2023)[90] measured an emission current of $0.586mA$ for NDD samples grown via MW-CVD on molybdenum substrates and terminated with hydrogen. This emission current was achieved at a temperature of $750°C$. Emission current measurements were taken using the same laser heating equipment (TEK) used in this work, the nitrogen and hydrogen layers were also grown in the same way. Therefore, any discrepancies in results must be due to the differences in absorber surfaces or the effects on the diamond surface of the absorber surface functionalisation.

The sample developed by Zulkharnay (2023)[90] had a laser-etched grating pattern micro-machined into the underside of the molybdenum substrate before diamond films were synthesised on the opposing surface of the sample. Gratings of this nature produce well-performing thermal absorbers, with some micro-structures reaching thermal absorbance of

Sample	Maximum Temperature $/^{\circ}C$	Maximum Emission Current $/mA$	Reference
NDSCD+H	1070	1.53 (mA/cm^2)	89
NDD+H	750	0.586	90
NDD+H	700	0.07 (mA/cm^2)	91
NDD+Sc	1100	3.1	90
NDD+OSn	700	2.0	27
NDD+OAl	900	0.05 (mA/cm^2)	91

Table 12: Shown here are the maximum emission currents and samples' maximum temperatures measured in various works, the source of each shown in the last column. Here, NDD and NDSCD represent nitrogen-doped diamond and nitrogen-doped single-crystal diamond respectively. Suffixes of '+x' denote the terminating species in keeping with the syntax of the rest of this written work. Emission values are displayed as found in their original works. Uncertain values displayed in this graph are visual estimates from graphical data, although these values are not accurate, they offer a rough point of reference for comparisons.

90% in the visible range.[92] Due to the time frame of this project and using methods available at this time, the DLC layer was grown as a pseudo-black-body absorber on the underside of the diamond sample as described in 2.3.i.

Due to the time constraints and maintenance of the MW-CVD reactor, the DLC layer had to be grown on the underside of the NDD sample post-diamond film growth. This seemingly did not affect the diamond layer which was to be expected due to the similar growth conditions of the absorber layer and diamond film.

However, upon the hydrogen termination of the sample, some visible changes in surface uniformity could be seen. Minimal damage had certainly been caused by the process in the centre of the sample in the form of what looked like delamination at the interface between the molybdenum substrate and the NDD film, although material remained on the surface so this was not full diamond delamination. Further investigation into the structure of the surface using scanning electron microscopy (SEM) would be useful here to fully determine any damage caused in detail. Damage to the surface of the sample, seemingly contained by the upper hydrogen-terminated layer, could have caused surface reconstruction of the NDD leading to fewer energetically favourable pathways of electrons for thermionic emission as a result of the change in crystal structure. This could simply mean non-uniform emission patterns (as seen in Figure 35 and Figure 36), or could lead to a lower threshold temperature and an increased operating temperature needed for optimal emission currents. The latter could explain the $\times 10$ reduction in maximum emission current found in this work and that found by Zulkharnay (2023)[90] for identically fabricated emission surfaces.

Due to the proposed lower WF of a lithium-terminated surface[91] the emission current of such a sample, especially with the aid of an NEA-promoting dopant such as nitrogen, was

hoped to be equal to, or even greater than, that of a hydrogen-terminated surface. The resulting emission current was five times smaller for an oxygen-lithium surface compared to the hydrogen surface.
Some amount of damage to the emission sample surface had occurred during the hydrogen terminating process, this sample underwent thermionic testing to high enough temperatures to desorb the hydrogen layer before being subject to a UVO-cleaner to treat the surface with atomic oxygen. In the next stages of the sample fabrication, it was subject to two more anneals at no higher temperature than $500°C$ and a lithium deposition via thermal evaporation (at $440°C$). Given the nature of these functionalisation steps, it is a reasonable assumption that no further damage was imparted on the surface, however, any existing surface damage would have remained as no new diamond layer was grown. If said damage was substantial enough, this could have impeded oxygen and hence lithium bonding to the surface. XPS analysis of this sample could indicate the strength of bonding to the diamond layer by assessing the attenuation of the oxygen peak towards the carbon peak. Changes in the structure of the oxygen-lithium layer may have led to different bonding configurations of the oxygen bond (ether and ketone) that have shown to affect WF and hence would impact the maximum possible emission current.[91] Weaker carbon-oxygen-lithium bonding would also accelerate the desorption process of the lithium-oxygen species, meaning the emission threshold temperature may not be reached without some level of desorption, especially if the WF of this layer has not been reduced as much as possible due to the affected atomic structure.

After the numerous heating cycles for thermal activation and measuring emission currents, some impairment to the absorber surface may have occurred. Although the DLC layer was made in a high-pressure, high-temperature environment, concentrated laser heating for prolonged periods may have damaged the area in which the laser was incident, this DLC had properties more akin to graphene than diamond so would not have the same structural or thermal resistance.
At the time of writing, the only comparisons for emission currents of oxygen- or alkali-terminated diamond samples were that of NDD+OSn[27] and NDD+OAL[91] (although, others have been theorised to perform well as thermionic emitters due to their large NEA, such as magnesium[93]). Thermionic results found in this work were twenty and five times lower than the aforementioned comparative samples respectively.

4 Conclusion

4.1 Future Work

In terms of future work for this project, there are a few ways in which the samples could be improved to yield higher emission currents. Functionalisation of the absorber surface with laser-etched gratings before diamond growth would produce non-damaged diamond films capable of greater thermal absorbance hence greater emission currents. Keeping samples under vacuum after lithium depositions and UPS measurements have been taken, whilst transferring the samples for thermionic emission testing would reduce contamination of the surfaces due to lithium's reactivity in air and produce emission currents representative of only the deposited surface species. X-ray photoemission spectroscopy analysis of samples exposed to air after full surface fabrication would investigate the full extent of this contamination and would determine whether the underlying oxygen layer stabilises the lithium layer.

A beta source could be added to the emitter surface to increase the electron population as well as the emission current.[94] Testing emission current with a radioactive heat source would also aid the investigation of the use of thermionic energy converters for extraterrestrial applications.

After this optimisation of the electron emitter, the collector surface of a thermionic energy converter could be developed. This would have to be a high-quality (low topography) sample with a lower work function than that of the emitter. Once these two surfaces have been fabricated, mitigation of the space-charge region that hinders electron emission can be investigated.

4.2 Concluding Remarks

In this study, functionalised diamond films were produced and tested primarily for their output emission currents as well as for estimations of their work functions. Nitrogen-doped diamond surfaces were grown on nucleated molybdenum using chemical vapour deposition, where two different nitrogen concentrations were investigated. Higher concentrations of nitrogen produced poorer-quality diamond films as a result of increased graphitic content. Fabricated surfaces were oxygenated using a UVO-cleaner and terminated with lithium by thermal evaporation in an ultra-high vacuum, two thicknesses of lithium were investigated. A set of four samples as described above were tested using ultraviolet photoemission spectrometry to estimate the position of their valence band maxima and work functions, samples were exposed to air for one week. Resulting work function estimations of the $0.3 sccm$ NDD samples were $-3.26eV$ and $-1.79eV$ for the HML and FML lithium coverages respectively.

These values give lower work functions than those found for comparable BDD+OLi samples found in literature[28,27]. Comparisons of the experimental values found in this work and theoretical values found by Martin (2011)[28] suggest that the higher quality, lower nitrogen concentration samples have oxygen arranged in the carbonyl position and lower quality, higher nitrogen concentration samples have oxygen in the ether position.
A singular $0.3sccm$ nitrogen-doped diamond sample had a diamond-like carbon layer grown on its absorber surface and was terminated with hydrogen using the CVD chamber and heated using an IR laser to measure the resulting emission current. This nitrogen concentration was chosen as it produced the highest-quality film out of the tested concentrations. After annealing the sample to remove the hydrogen layer, the surface was treated with oxygen and HML coverage of lithium before undergoing thermionic emission testing once more. This thickness was chosen as it was theorised to give the lowest work function so would yield the best emission current. Maximum emission currents found for hydrogen and oxygen-lithium terminated $0.3sccm$ NDD samples were $0.051mA$ and $0.016mA$ respectively. Emission was lower than expected for both types of terminations, comparable NDD+H samples in literature[89] were ten times larger. The dependence on the work function of a specific lithium coverage and the bonding configuration of the underlying oxygen layer has been studied by others[28] and may explain why the expected emission from a HML lithium coverage was greater than achieved.
Producing low-work function materials is crucial for the fabrication of effective emitter and collector surfaces to be used as electrodes in a complete thermionic converter device. Such a device has a plethora of applications, arguably the most important of these being renewable and clean energy production as well as clean hydrogen production by electrolysis. More aspirational applications of such a device include space-based solar power and power generation for space exploration using a radioactive heat source.
In the scope of this work the combination of lithium, oxygen and nitrogen for diamond thermionics has been successful. Despite various factors discussed in this work that have affected the maximum emission currents available in the fabricated samples, emission has been achieved with room for improvement in terms of sample quality and absorber surface functionalisations. Although work function measurements can only be made with some amount of accuracy, they do suggest that incorporating nitrogen into the diamond film, as opposed to boron, is successful in further reducing the work function of oxygen-lithium terminated diamond. These tests were also carried out on undamaged samples to give a glimpse of the potential of such samples if thermionic emission testing were to take place. Emission currents from the NDD+OLi sample (38) were very stable across all six cycles, a great improvement on the irregular currents generated by similar diamond films terminated with only hydrogen. All of these factors investigated throughout this work have succeeded in demonstrating the great potential of lithium-oxide nitrogen-doped diamond films

as thermionic emitter surfaces.

References

[1] K.M.O'Donnell, T.L.Martin, N.A.Fox, and D.Cherns. *Ab Initio Investigation of Lithium on the Diamond C(100) Surface*. *Physical Review*, **82**, 2010.

[2] S.Ullah, L.Cullingford, T.Zhang, J.R.Wong, G.Wan, M.Cattelan, and N.Fox. *An Investigation into the Surface Termination and Near-Surface Bulk Doping of Oxygen-Terminated Diamond with Lithium at Various Annealing Temperatures*. *MRS Advances*, **6**, 2021.

[3] S.Ullah, G.Wan, C.Kouzios, C.Woodgate, M.Cattelan, and N.Fox. *Structure and Electronic Properties of Tin Monoxide (SnO) and Lithiated SnO Terminated Diamond (100) and its Comparison with Lithium Oxide Terminated Diamond. Applied Surface Science*, **559**, 2021.

[4] M.C.Salvadori, W.W.R.Araujo, F.S.Teixeria, N.Cattani, A.Pasquarelli, E.M.Oks, and I.G.Brown. *Termination of Diamond Surfaces with Hydrogen, Oxygen and Fluorine Using a Small, Simple Plasma Gun*. *Diamond and Related Materials*, **19**:234–328, 2010.

[5] N.Donato, N.Rouger, J.Pernot, G.Longobardi, and F.Udrea. *Diamond Power Devices: State of the Art, Modelling, Figures of Merit and Future Perspective*. *Journal of Physics D: Applied Physics*, 53, 2020.

[6] G.R.Mackenzie, S.Kaluvan, P.G.Martin, C.Hutson, T.Connolley, M.Cattelan, H.Dominguez-Andrade, T.L.Martin, N.A.Fox, and T.B.Scott. *A Diamond Gammavoltaic Cell Utilizing Surface Conductivity and its Response to Different Photon Interaction Mechanisms*. *Materialstoday: Energy*, 21, 2021.

[7] D.B.Go, J.R.Haase, J.George, J.Mannhart, R.Wanke, A.Nojeh, , and R.Nemanich. *Thermionic Energy Conversion in the Twenty-first Century: Advances and Opportunities for Space and Terrestrial Applications*. *Frontiers in Mechanical Engineering*, 3, 2017.

[8] M.C.James, F.Fogarty, R.Zulkharnay, N.A.Fox, and P.W.May. *A Review of the Surface Functionalisation of Diamond for Thermionic Carbon*. *Carbon*, **171**:532–550, 2021.

[9] C.E.Nebel and J.Ristein. *Semiconductors and Semimetals: Thin Film Diamond II*. *Elsevier Academic Press*, 77, 2004.

[10] D.Y.Liu, L.C.Hao, Y.Teng, F.Qin, Y.Shen, K.Tang andJ.D.Ye, S.M.Zhu, R.Zhang, Y.D.Zheng, and S.L.Gu. *Nitrogen Modulation of Boron Doping Behavior for Accessible N-Type Diamond*. *APL Materials*, 9, 2021.

[11] A.Croot. *Boron and Nitrogen in Diamond: An Ab Initio Simulation, Plasma Emission Spectroscopy and Material Deposition and Characterisation Study*. PhD thesis, 2018.

[12] M.Kosowska, S.Pawłowska, K.J.Sankaran, D.Majchrowicz, K.Haenen, K.Dholakia, and M.Szczerska. *Incorporation of Nitrogen in Diamond Films – A New Way of Tuning Parameters for Optical Passive Elements*. *Diamond and Related Materials*, 111, 2021.

[13] A.M.Zaitsev, N.M.Kazuchits, V.N.Kazuchits, K.S.Moe, M.S.Rusetsky, O.V.Korolik, K.Kitajima, J.E.Butler, and W.Wang. *Nitrogen-Doped CVD Diamond: Nitrogen Concentration, Color and Internal Stress*. *Diamond and Related Materials*, 105, 2020.

[14] A.Croot, M.Z.Othman, S.Conejeros, N.A.Fox, and N.L.Allan. A theoretical study of substitutional boron-nitrogen clusters in diamond. *Journal of Physics: Condensed Matter*, **30**, 2018.

[15] D.Y.Liu, L.C.Hao, Y.Teng, F.Qin, Y.Shen, K.Tang, J.D.Ye, R.Zhang S.M.Zhu, Y.D.Zheng, and S.L.Gu. *Nitrogen Modulation of Boron Doping Behavior for Accessible N-Type Diamond*. *APL Materials*, **9**, 2021.

[16] S.Conejeros, M.Z.Othman, A.Croot, J.N.Hart, K.M.O'Donnell, P.W.May, and N.L.Allan. *Hunting the Elusive Shallow N-Type Donor – an Ab Initio Study of Li and N Co-Doped Diamond*. *Carbon*, **171**, 2020.

[17] M.N.R.Ashfold, J.P.Goss, B.L.Green, P.W.May, M.E.Newton, and C.V.Peaker. *Nitrogen in Diamond*. *Chemical Review*, **120**, 2020.

[18] S.Orlanducci, A.Fiori, V.Sessa, E.Tamburri, F.Toschi, and M.L.Terranova. *Nanocrystalline Diamond Films Grown in Nitrogen Rich Atmosphere: Structural and Field Emission Properties*. *Nanoscience and Nanotechnology*, **8**, 2008.

[19] E.Staryga, K.Fabisiak, M.Dłużniewski, and G.W.Bąk. *Electron Emission from Nitrogen-Doped Polycrystalline Diamond/Si Heterostructures*, journal = Materials Science Poland, issue = 30, volume = 4. 2012.

[20] J.Garai. *Electron Configuration of the Substitutional Nitrogen Defect in Diamond*.

[21] R.Li. *A Molecular Dynamics Study of Boron and Nitrogen in Diamond*. *Solid State Communications*, **135**, 2005.

[22] Y.Nakano, X.Zhang, K.Kobayashi, T.Matsumoto, T.Inokuma, S.Yamasaki, C.E.Nebel, and N.Tokuda. *Impact of Nitrogen Doping on Homoepitaxial Diamond (111) Growth*. *Diamond and Related Materials*, **125**, 2022.

[23] V.Baranauskas, B.B.Li, A.Peterlevitz, M.C.Tosin, and S.F.Durrant. *Nitrogen-Doped Diamond Films*. *Journal of Applied Physics*, **85**:7455–7458, 1999.

[24] K.J.Sankaran. *Fabrication, Microstructure, and Enhanced Thermionic Electron Emission Properties of Vertically Aligned Nitrogen-Doped Nanocrystalline Diamond Nanorods*. *MRS Communications*, 8, 2018.

[25] M.A.Lobaev, A.M.Gorbachev, S.A.Bogdanov, A.L.Vikharev, D.B.Radishev, V.A.Isaev, V.V.Chernov, and M.N.Drozdov. *Influence of CVD Diamond Growth Conditions on Nitrogen Incorporation*. *Diamond and Related Materials*, 72:1–6, 2017.

[26] M.Kataoka, C.Zhu, F.A.M.Koeck, and R.J.Nemanich. *Thermionic Electron Emission from Nitrogen-Doped Homoepitaxial Diamond*. *Diamond and Related Materials*, 19:110–113, 2010.

[27] S.Ullah. *Sustainable Functionalization of Diamond Surface with Tin, Lithium, and Oxygen For Low Work Function Applications*. PhD thesis, University of Bristol, 2023.

[28] T.L.Martin. *Lithium Oxygen Termination as a Negative Electron Affinity Surface on Diamond: a Computational and Photoemission Study*. PhD thesis, 2011. PhD Thesis.

[29] F.A.M.Koeck and R.J.Nemanich. *Low Temperature Onset for Thermionic Emitters Based on Nitrogen Incorporated UNCD Films*. *Diamond and Related Materials*, **18**:232–234, 2009.

[30] F.A.M.Koeck and R.J.Nemanich. *Substrate-Diamond Interface Considerations for Enhanced Thermionic Electron Emission from Nitrogen Doped Diamond Films*. *Journal of Applied Physics*, **112**:113707, 2012.

[31] W.F.Paxton, M.Howell, W.P.Kang, and J.L.Davidson. *Influence of Hydrogen on the Thermionic Electron Emission from Nitrogen-Incorporated Polycrystalline Diamond Films*. *Journal of Vacuum Science and Technology B*, **30**, 2012.

[32] F.A.M.Koeck and R.J.Nemanich. *Emission Characterization from Nitrogen-Doped Diamond With Respect to Energy Conversion*. *Diamond and Related Materials*, **15**:217–220, 2006.

[33] F.A.M.Koeck and R.J.Nemanich. *Advances in Thermionic Energy Conversion Through Single-Crystal N-Type Diamond*. *Frontiers of Mechanical Engineering*, **3**:1–11, 2017.

[34] M.Kataoka, C.Zhu, F.A.M.Koeck, and R.J.Nemanich. *Thermionic Electron Emission from Nitrogen-Doped Homoepitaxial Diamond*. *Diamond and Related Materials*, **19**:110–113, 2010.

[35] H.Kato, D.Takeuchi, M.Ogura, T.Yamada, M.Kataoka, Y.Kimura, S.Sobue, C.E.Nebel, and S.Yamasaki. *Heavily Phosphorus-Doped Nano-Crystalline Diamond Electrode for Thermionic Emission Application*. *Diamond and Related Materials*, **63**:165–168, 2016.

[36] K.M.O'Donnell, T.L.Martin, M.T.Edmonds, A.Tadich, L.Thomsen, J.Ristein, C.I.Pakes, N.A.Fox, and L.Ley. *Photoelectron Emission from Lithiated Diamond*. *Physica Status Solidi*, 211:2209–2222, 2014.

[37] Z.Sun, M.Yang, X.Wang, P.Wang, C.Zhang, N.Gao, and H.Li. *Boron-Terminated Diamond (100) Surfaces with Promising Structural and Electronic Properties*. *Physical Chemistry and Chemical Physics*, 22:8060–8066, 2020.

[38] M.C.James, A.Croot, P.W.May, and N.L.Allan. *Negative Electron Affinity from Aluminium on the Diamond (100) Surface: A Theoretical Study*. *Journal of Physics: Condensed Matter*, 30:235002, 2018.

[39] J.Van Der Weide, Z.Zhang, P.K.Baumann, M.G.Wensell, J.Bernholc, and R.J.Nemanich. *Negative-Electron-Affinity Effects on the Diamond (100) Surface*. 50:5803–5806, 1994.

[40] J.Furthmüller, J.Hafner, and G.Kresse. *Surface Reconstruction and Electronic Properties of Clean and Hydrogenated Diamond (111) Surfaces*. *Physical Review B*, 53:7334–7351, 1996.

[41] M.J.Rutter and J.Robertson. *Ab Initio Calculation of Electron Affinities of Diamond Surfaces*. *Physical Review B*, 57:9241–9245, 1998).

[42] W.Shen, Y.Pan, S.Shen, H.Li, Y.Zhan, and G.Zhang. *Electron Affinity of Boron-Terminated Diamond (001) Surfaces: A Density Functional Theory Study*. *Journal of Physics: Condensed Matter*, 7:9756–9765, 2019.

[43] M.J.Sear, A.K.Schenk, A.Tadich, A.Stacey, and C.I.Pakes. *P-Type Surface Transfer Doping of Oxidised Silicon Terminated (100) Diamond*. *Applied Physics Letters*, 110, 2017.

[44] M.C.James, P.W.May, and N.L.Allan. *Ab Initio Study of Negative Electron Affinity from Light Metals on the Oxygen-Terminated Diamond (111) Surface*. *Journal of Physics: Condensed Matter*, **31**:295002, 2019.

[45] K.M.O'Donnell, T.L.Martin, and N.L.Allan. *Light Metals on Oxygen-Terminated Diamond (100): Structure and Electronic Properties*. *Chemistry of Materials*, **27**:1306–1315, 2015.

[46] J.Navas, D.Araujo, J.C.Piñero, A.Sánchez-Coronilla, E.Blanco, P.Villar, R.Alcántara, J.Montserrat, M.Florentin, D.Eon, and J.Pernot. *Oxygen Termination of Homoepitaxial Diamond Surface by Ozone and Chemical Methods: An Experimental and Theoretical Perspective*. *Applied Surface Science*, **433**:408–418, 2018.

[47] H.O.Pierson. *HANDBOOK OF CARBON, GRAPHITE, DIAMOND and FULLERENES: Properties, Processing and Applications*. Noyes Publications, 1994.

[48] Diamond Materials. *Thermal Properties of CVD Diamond*. https://www.diamond-materials.com/en/cvd-diamond/thermal/. Date Accessed: 14/07/23.

[49] Lambda Geeks: A.Mapari. *Does Graphene Conduct Electricity? 11 Facts (How, Why and Uses)*. https://lambdageeks.com/does-graphene-conduct-electricity/?utm_content=cmp-true. Date Accessed: 14/07/23.

[50] M.Sang, J.Shin, K.Kim, and K.J.Yu. *Electronic and Thermal Properties of Graphene and Recent Advances in Graphene Based Electronics Applications*. *Nanomaterials*, 9, 2019.

[51] Physics World. *Tuning the Gap in Graphene*. https://physicsworld.com/a/tuning-the-gap-in-graphene/. Date Accessed: 14/07/23.

[52] ThoughtCo. *Table of Electrical Resistivity and Conductivity*. https://www.thoughtco.com/table-of-electrical-resistivity-conductivity-608499. Date Accessed: 14/07/23.

[53] Material Properties. *Silicon*. https://material-properties.org/Silicon-thermal-properties-melting-point-thermal-conductivity-expansion/. Date Accessed: 14/07/23.

[54] Virginia Semiconductor. *The General Properties of Si, Ge, SiGe, SiO_2 and Si_3N_4*, 2002.

[55] TOSHIBA. *What is a Wide-Band-Gap Semiconductor?* https://toshiba.semicon-storage.com/apen/semiconductor/knowledge/faq/diode_sic-sbd/sic-sbd001.html. Date Accessed: 14/07/23.

[56] ThoughtCo. *Electrical Conductivity of Metals*. https://www.thoughtco.com/electrical-conductivity-in-metals-2340117: :text=Date Accessed: 14/07/23.

[57] Material Properties. *Molybdenum*. https://material-properties.org/molybdenum-thermal-properties-melting-point-thermal-conductivity-expansion/. Date Accessed: 14/07/23.

[58] CK-12. *25.1 Carbon, A Unique Element*, 2012. Date Accessed: 31/10/22.

[59] J.R.Siqueira Jr.and O.N.Oliveira Jr. *Nanostructures, Chapter = 9-Carbon-Based Nanomaterials*. William Andrew: Applied Science Publishers, 2017.

[60] BYJU'S. *Fermi Energy*. https://byjus.com/physics/fermi-energy/. Date Accessed: 10/22.

[61] BYJU'S. *Magnetic Quantum Number*. https://byjus.com/physics/magnetic-quantum-number/. Date Accessed: 10/22.

[62] R.Nave: HyperPhysics. *Fermi Energy*. Date Accessed: 10/22.

[63] R.Nave: HyperPhysics. *Semiconductor Energy Bands*. Date Accessed: 10/22.

[64] R.J.Nemanich, P.K.Baumann, M.C.Benjamin, S.W.King, J.van der Weide, and R.F.Davis. *Negative Electron Affinity Surfaces of Aluminum Nitride and Diamond*. *Diamond and Related Materials*, 5:790–796, 1996.

[65] K.P.Loh, I.Sakaguchi, M.Nishitani-Gamo, T.Taniguch, and T.ando. *Negative Electron Affinity of Cubic Boron Nitride*. *Diamond and Related Materials*, 8:781–784, 1999).

[66] O.E.Tereshchenko, V.A.Golyashov, A.A.Rodionov, I.B.Chistokhin, N.V.Kislykh, A.V.Mironov, and V.V.Aksenov. *Solar Energy Converters Based on Multi-Junction Photoemission Solar Cells*. *Nature Scientific Reports*, 7, 2017.

[67] J.S.Escher. *Semiconductors and Semimetals*, volume 15. 1981.

[68] SZ.Zhang and J.T.Yates Jr. *Band Bending in Semiconductors: Chemical and Physical Consequences at Surfaces and Interfaces*. *Chemical Reviews*, **10**:5520–5551, 2012.

[69] University of Cambridge. *Metal-Semiconductor Junction - Rectifying Contact*. https://www.doitpoms.ac.uk/tlplib/semiconductors/junction$_r ectifying.php.DateAccessed$: 15/02/23.

[70] H.Ibach. *Physics of Surfaces and Interfaces*. Springer, 2006.

[71] LibreTexts Chemistry. *Physical and Theoretical Chemistry: Ionization Energy*. https://chem.libretexts.org/Bookshelves/, 2023. Date Accessed: 08/02/23.

[72] J.Clark: ChemGuide. *Electron Affinity*. https://www.chemguide.co.uk/atoms/properties/eas.html, 2021. Date Accessed: 08/02/23.

[73] R.Nave: HyperPhysics. *The Doping of Semicnoductors*. Date Accessed: 10/22.

[74] L.Schachter, K.E.Stiebing, and S.Dobrescu. *On the Role of Electron Energy Distribution Function in Double Frequency Heating of Electron Cyclotron Resonance Ion Source Plasmas*. *Review of Scientific Instruments*, 85, 2014.

[75] J.M.Houston. *Theoretical Efficiency of the Thermionic Energy Converter*. *Journal of Applied Physics*, 30, 1959.

[76] F.A.M.Koeck, R.J.Nemanich, and J.Sharp. *Doped Diamond Thin Film Electron Sources for Thermionic Energy Conversion*. *26^{th} International Vacuum Nanoelectronics Conference (IVNC)*, 2013.

[77] W.F.Paxton, S.Ravipati, M.M.Brooks, M.Howell, and J.L.Davidson. *Thermionic Emission from Diamond Films in Molecular Hydrogen Environments*. *Frontiers of Mechanical Engineering*, 3, 2017.

[78] F.A.M.Koeck, R.J.Nemanich, Y.Balasubramaniam, and K.Haenenand J.Sharp. *Enhanced Thermionic Energy Conversion and Thermionic Emission from Doped Diamond Films Through Methane Exposure*. *Diamond and Related Materials*, 20, 2011.

[79] S.Ullah and N.Fox. *Modification of the Surface Structure and Electronic Properties of Diamond (100) with Tin as a Surface Termination: A Density Functional Theory Study. J.Phys.Chem.C*, **125**:25165–25174, 2021.

[80] O.J.L.Fox, J.O.P.Holloway, G.M.Fuge, P.W.May, and M.N.R.Ashfold. *Electrospray Deposition of Diamond Nanoparticle Nucleation Layers for Subsequent CVD Diamond Growth*. *MRS Online Proceedings Library volume*, **1203**, 2009.

[81] P.May. *CVD Diamond - a New Technology for the Future? Endevour Magazine*, **19**, 1995.

[82] S.Ullah, G.Wan, C.Kouzios, C.Woodgate, M.Cattelan, and N.A.Fox. *Structure and Electronic Properties of Tin Monoxide (SnO) and Lithiated SnO Terminated Diamond (100) and its Comparison with Lithium Oxide Terminated Diamond*. *Applied Surface Science*, (149962), 2021.

[83] M.Fowkes. *Attractive Forces at Interface*. *Industrial and Engineering Chemistry*, **56**:40–52, 1964.

[84] SEAS Soft Matter Wiki. *Adsorption*. http://soft-matter.seas.harvard.edu/index.php/Adsorption, 2012. Date Accessed: 08/02/23.

[85] Materials Square. *Adsorption Energy and Surface Energy Obtained through Slab Structure*. https://www.materialssquare.com/blog/10-adsorption-energy- and-surface-energy-obtained-through-slab-structure, 2019. Date Accessed: 07/02/23.

[86] XPS Fitting. *Thickogram*. https://www.xpsfitting.com/2009/04/thickogram.html. Date Accessed: 03/08/23.

[87] H.Cen, S.Nunez-Sanchez, I.Bickerton, N.A.Fox, and M.J.Cryan. *Solar Thermal Characterisation of Micro-Patterned High Temperature Selective Surfaces*. *Journal of Photonics for Energy*, **10**, 2020.

[88] G.Kim, H.Kim, B.Walker, H.Choi, C.Yang, J.Park, and J.Y.Kim. *Effects of Ionic Liquid Molecules in Hybrid PbS Quantum Dot–Organic Solar Cells*. *ACS: Applied Materials and Interfaces*, 5:1757–1760, 2013.

[89] H.Dominguez-Andrade, J.Anaya, A.Croot, M.Cattelan, D.J.Twitchen, M.Kuball, and N.A.Fox. *Correlating Thermionic Emission with Specific Surface Reconstructions in a <100> Hydrogenated Single-Crystal Diamond*. *ACS Applied Materials and Interfaces*, **12**, 2020.

[90] R.Zulkharnay. *Electron Emission Studies of Scandium on Diamond for Thermionic Solar Energy Generation Devices*. PhD thesis, University of Bristol, 2023.

[91] M.C.James. *Aluminium and Oxygen Termination of Diamond for Thermionic Applications*. PhD thesis, University of Bristol, 2019.

[92] S.Nunez-Sanchez, H.D.Andrade, J.Harwood, I.Bickerton, N.A.Fox, and M.J.Cryan. *Molybdenum Gratings as a High-Temperature Refractory Platform for Plasmonic Heat Generators in the Infrared*. *Micro and Nano Letters*, **13**, 2018.

[93] K.M.O'Donnell, M.T.Edmonds, A.Tadich, L.Thomsen, A.Stacey, A.Schenk, C.I.Pakes, and L.Ley. *Extremely High Negative Electron Affinity of Diamond via Magnesium Adsorption*. *Cornell University: ArXiv 1505.06410*, 2015.

[94] A.Croot, G.Wan, A.Rowan, H.D.Andrade, J.A.Smith, and N.A.Fox. *Beta Radiation Enhanced Thermionic Emission from Diamond Thin Films*. *Frontiers in Mechanical Engineering*, 3, 2017.

5 Appendix

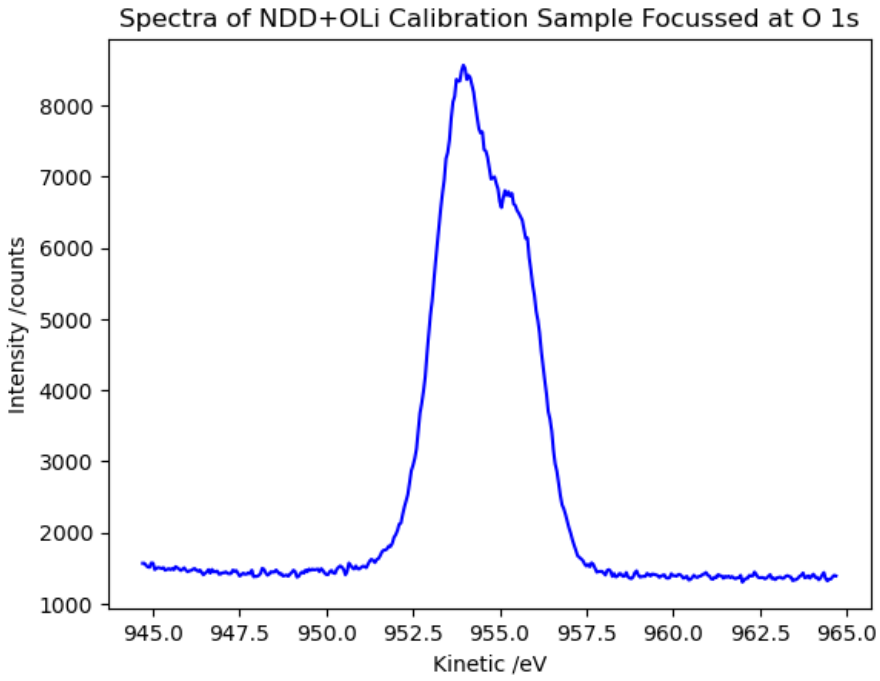

Figure 39: Spectra obtained for an electrostaticaly nucleated 0.3sccm NDD sample terminated with ML coverage of oxygen via UV-ozone exposure, terminated with lithium at 440°C.

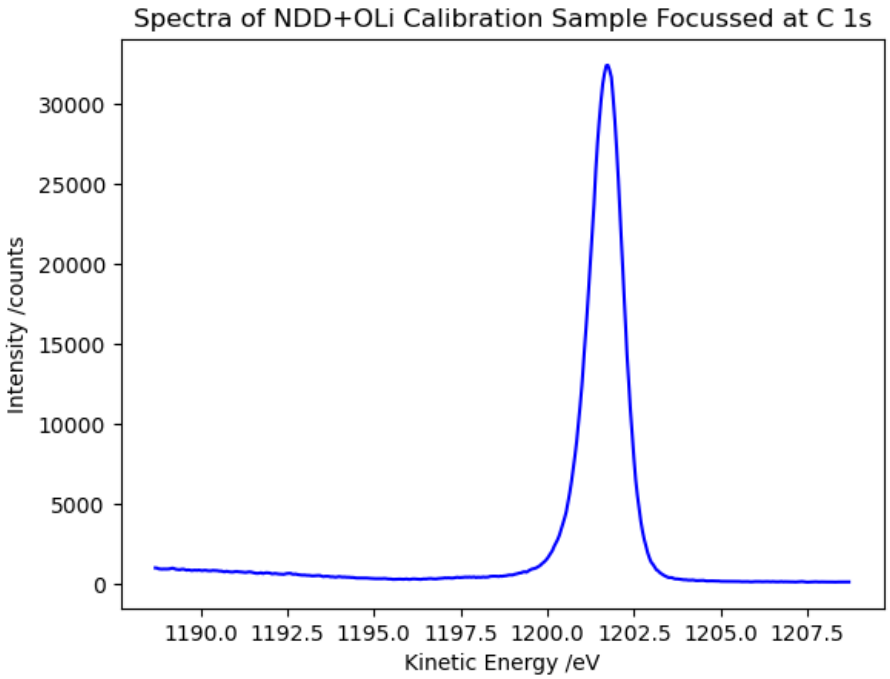

Figure 40: Spectra obtained for an electrostatically nucleated 0.3sccm NDD sample terminated with ML coverage of oxygen via UV-ozone exposure, terminated with lithium at 440°C.

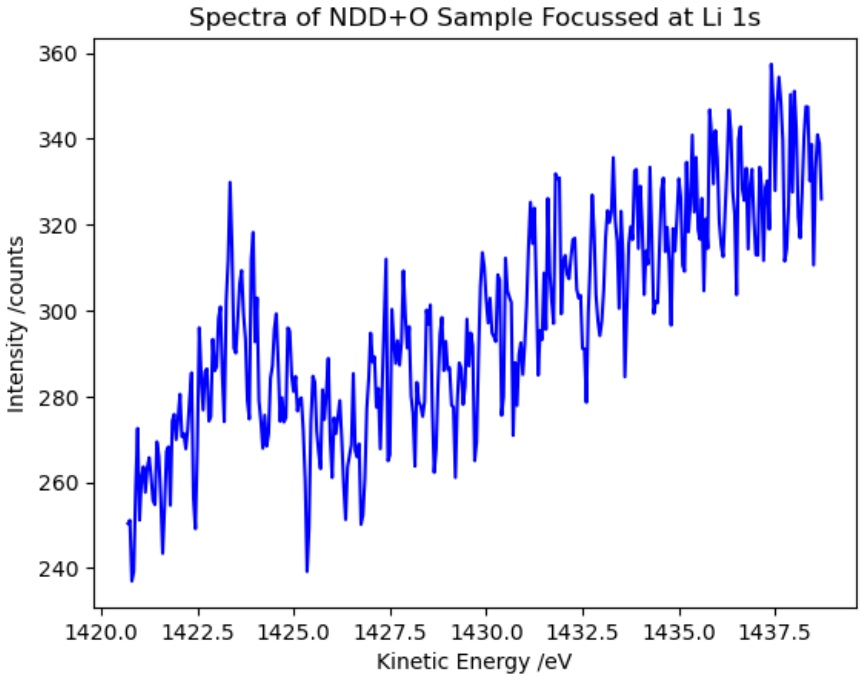

Figure 41: Spectra obtained for an electrostaticaly nucleated 0.3sccm NDD sample terminated with ML coverage of oxygen via UV-ozone exposure.

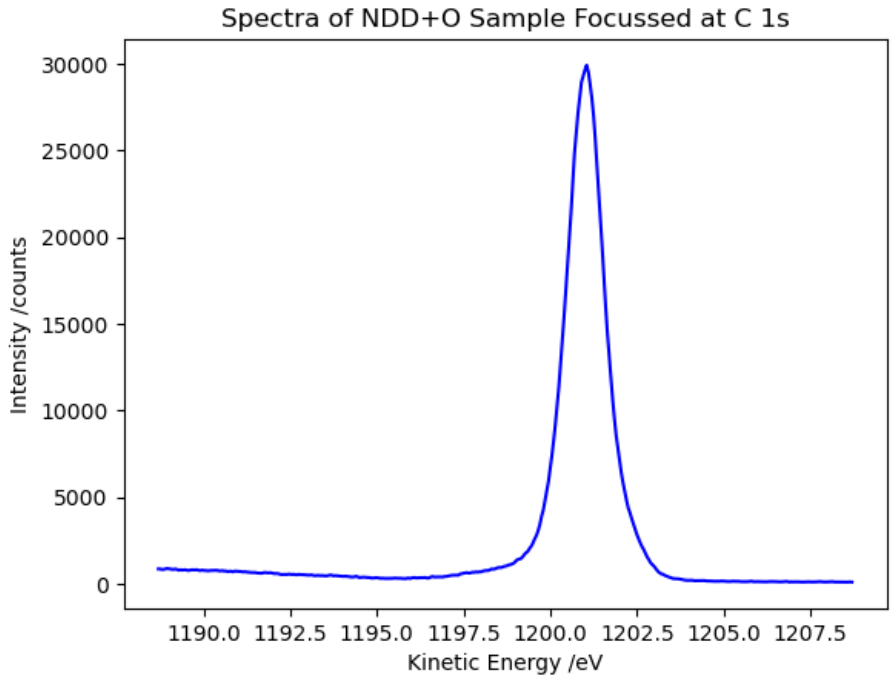

Figure 42: Spectra obtained for an electrostatically nucleated 0.3sccm NDD sample terminated with ML coverage of oxygen via UV-ozone exposure

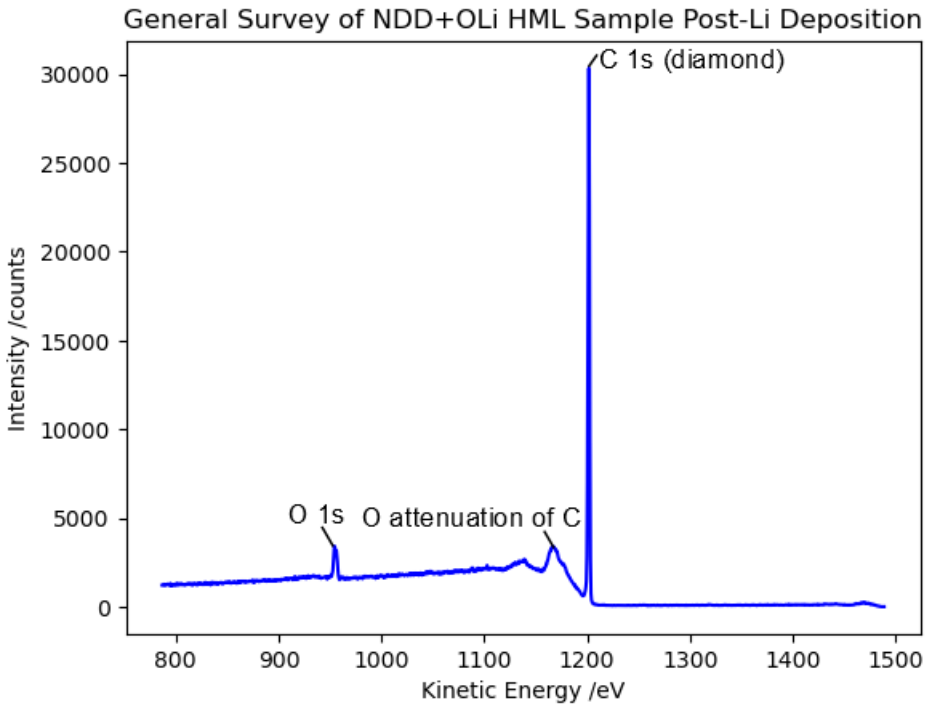

Figure 43: General survey of an electrostatically nucleated 0.3sccm NDD sample terminated with ML coverage of oxygen via UV-ozone exposure, terminated with HML coverage of lithium at 440°C and annealed for 1 hour at 500°C

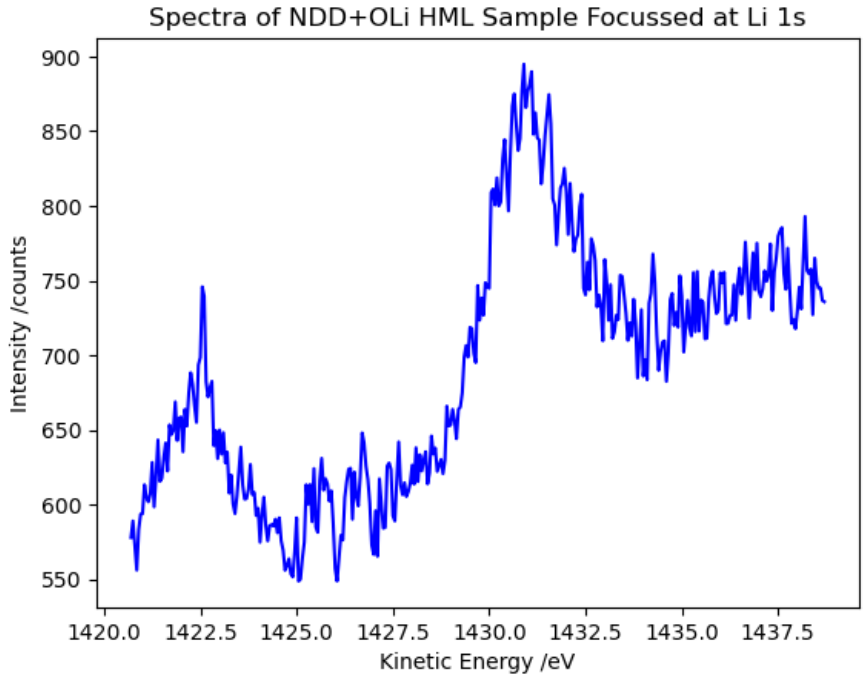

Figure 44: Spectra obtained for an electrostaticaly nucleated 0.3sccm NDD sample terminated with ML coverage of oxygen via UV-ozone exposure, terminated with HML coverage of lithium at 440°C.

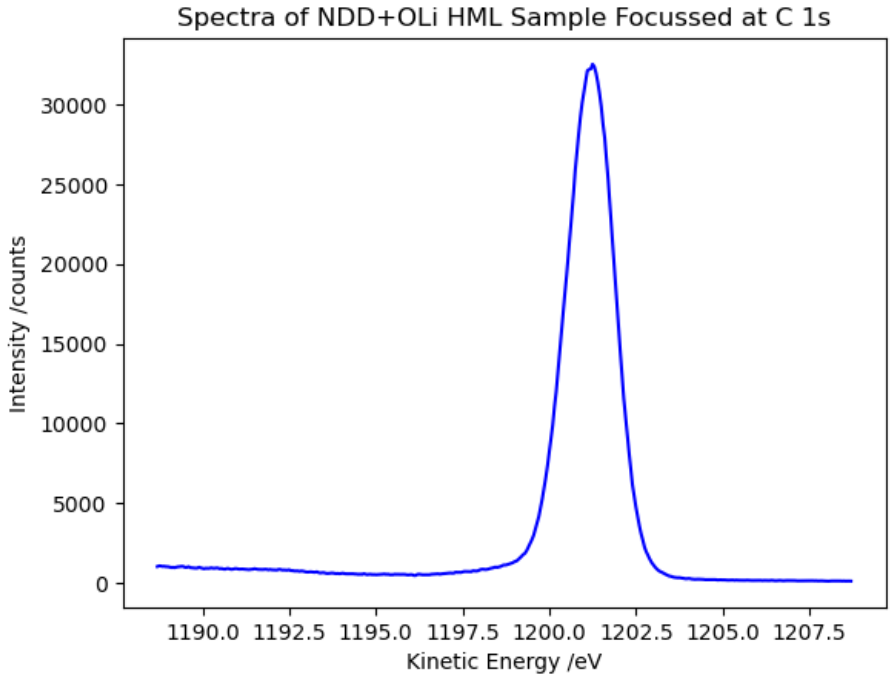

Figure 45: Spectra obtained for an electrostatically nucleated 0.3sccm NDD sample terminated with ML coverage of oxygen via UV-ozone exposure, terminated with HML coverage of lithium at 440°C.